Available online at www.sciencedirect.com
ScienceDirect
International Journal of Heat and Fluid Flow 29 (2008) 427–448
International Journal of HEAT AND FLUID FLOW
www.elsevier.com/locate/ijhff

# Modelling of high-pressure dense diesel sprays with adaptive local grid refinement

S. Tonini [a,1], M. Gavaises [a,*], A. Theodorakakos [b]

[a] School of Engineering and Mathematical Sciences, City University London, UK
[b] Fluid Research Co., Athens, Greece

Received 2 May 2007; received in revised form 29 October 2007; accepted 23 November 2007
Available online 8 February 2008

**Abstract**

An Eulerian–Lagrangian fluid dynamics model simulating the development of dense liquid plumes formed during injection of fuels against compressed air is described and assessed against experimental data. The numerical model employs an adaptive local grid refinement methodology combined with a calculation procedure distributing the mass, momentum and energy exchanged between the liquid and gaseous phases in the numerical cells found in the vicinity of the moving droplets. The use of appropriate weighting functions resolves numerical as well as physical problems realised when the interaction volume available between the two phases is limited to the cell-containing parcel, whose volume may become comparable to that of the dispersed phase. Calculation of 'virtual' cell properties provide better estimates for the flow variables realised by the droplets crossing cells in the wake of those upstream and allows for larger time steps to be employed in the solution of the carrier phase conservation equations. The results suggest that the proposed methodology offers significant improvements compared to the standard Lagrangian one frequently adopted in simulation of combustion systems, without the need to use Eulerian flow models in dense spray regions.


*Keywords:* Eulerian–Lagrangian methodology; Adaptive mesh refinement; Dense Diesel spray

## 1. Introduction

Within the last decade, the direct injection Diesels and more frequently the close-spacing spray-guided direct injection gasoline combustion systems have become the most popular engines for modern passenger car applications. It is generally accepted now that complicated injection strategies are required. These involve the use of high-pressure injection systems employing multiple injections during the engine cycle. Experiments have shown that the duration of these injections and the spacing between them are required to be very small in order to reach the desired reduction in emissions. Electronic control technology is now available to operate the injection equipment at these levels offering advantages in combustion advantages. CFD (Computational Fluid Dynamics) has become an integral part of the analysis and design of automotive products. Effective models, which provide cost efficient ways of studying different engine geometries, operating conditions and injection strategies are essential tools in modern engine design since they reduce the number of experimental test cases required for product development, as reported by Canakci and Reitz (2003). Simulation of the airflow development inside the inlet/exhaust manifold as well as inside the engine cylinder requires a mesh with cell size of the order of $10^{-3}$ m and a time step of about $10^{-3}$ s. On the other hand, the processes governing the fuel injection system should be predicted using smaller time steps of the order of $10^{-8}$ s in much finer computational grids, which cell size varies from $10^{-4}$ m for in-cylinder spray development investigation, down to $10^{-6}$ m for internal nozzle flow and liquid atomisation

* Corresponding author. Tel.: +44 2070408115; fax: +44 2070408566.
*E-mail address:* m.gavaises@city.ac.uk (M. Gavaises).
[1] Present address: Industrial Engineering Department, Università di Bergamo, Italy.

0142-727X/$ - see front matter © 2007 Elsevier Inc. All rights reserved.
doi:10.1016/j.ijheatfluidflow.2007.11.009

**Nomenclature**

*Greek symbols*

| | |
|---|---|
| $\alpha$ | volume fraction |
| $\delta$ | distribution weighting factor |
| $\Delta l$ | control volume reference length |
| $\Delta t$ | time step |
| $\varepsilon$ | kinetic energy dissipation rate |
| $\varphi$ | scalar variable |
| $\gamma$ | constant of proportionality |
| $\lambda$ | interpolation/distribution method proportionality factor |
| $\rho$ | density |
| $\sigma\delta$ | standard deviation |
| $\Psi$ | interpolation/distribution method parameter |
| $\tau$ | non-dimensional time |

*Roman symbols*

| | |
|---|---|
| $A_1$ | constant of proportionality |
| $C_p$ | heat capacity at constant pressure |
| $CN$ | Courant Number |
| dist | parcel-to-cell relative distance |
| $D$ | diameter |
| $f$ | function |
| $m$ | mass |
| $N$ | number |
| $P$ | pressure |
| $r$ | interpolation distance |
| $R$ | radius |
| $\mathbf{s}$ | source terms |
| sp | spray penetration |
| $t$ | time |
| $T$ | temperature |
| $u$ | velocity vector module |
| $\mathbf{u}$ | velocity vector |
| $V$ | volume |
| $\mathbf{x}$ | spatial coordinate vector |

*Subscripts*

| | |
|---|---|
| atom | atomisation |
| back | back conditions |
| break | break-up |
| C | continuous phase |
| coll | collision/coalescence |
| i | index |
| inj | injection |
| interp/dist | interpolation/distribution distance |
| l | liquid |
| max | maximum |
| p | particle |
| P | dispersed phase parcel |
| turb | turbulence |
| v | vapour |

*Superscripts*

| | |
|---|---|
| new | current time step |
| old | old time step |
| – | experimental value |

predictions, respectively. Furthermore, the fuel injection time interval corresponds to a small fraction of the total engine cycle. Its duration lasts for few engine crank angles and it is usually modelled using a time step of the order of $10^{-5}$ s. The accuracy of CFD simulations is determined not only by the adequacy of the physical models but also from the dependency of the results on the discretisation techniques implemented, which may suffer of accuracy and stability problems, as reported for example, by Schmidt and Rutland (2003). In the literature, extensive investigations on adequate scaling factors in order to compensate for the mesh influence have been presented, emphasising the necessity to empirically tune coefficients or other inputs to the models by reference to experimental data to obtain satisfactory predictions (Gosman, 1999). It is generally accepted that accurate modelling of the interaction of flows with sprays is a key factor in simulating the whole engine flow and combustion process. The most commonly used CFD codes employ the stochastic particle method of Dukowicz (1980), to account for the dispersed phase on a Lagrangian frame of reference, where the properties of the representative droplet parcels are randomly chosen from empirical or calculated distribution functions. With this methodology, phenomenological sub-models are required to account for the various physical processes taking place in the sub-grid time and length scales. Nowadays the physical sub-models predicting the spray processes are still limited to specific flow conditions, thus, empirical to some extent (Lippert et al., 2005). The processes controlling the fuel spray development include a variety of parameters like the nozzle geometry, the characteristics of the fuel supply system and the liquid–gas aerodynamic interaction. Particular emphasis has been given in the last decade to the influence of the temporal and spatial resolution of the continuous air motion on the computational spray sub-models. Many studies have demonstrated the strong dependence of the method on the grid resolution, for example Abraham (1997), Subramaniam and O'Rourke (1998) and Lippert et al. (2005), among others. The reason for such grid-dependence is that, on one hand, the volume of the cells introduced for the discretisation of the gas phase equations should be bigger than the volume of the droplets they contain, as imposed by the Eulerian–Lagrangian formulation, on the other hand, the grid size should be small enough to accurately resolve the gas phase development near the nozzle. These contradictory requirements are not easily

satisfied at operating conditions of high pressure Diesel and gasoline sprays. Moreover, Aneja and Abraham (1998) have concluded that grid dependency is influenced by the various sub-models involved. Lippert et al. (2005) distinguished the phase coupling into 'gas-to-liquid' and 'liquid-to-gas'. The first comprises the interpolation process, whereby gas quantities known at Eulerian nodes are estimated at the parcel location. Liquid-to-gas coupling refers to the summation of particle source terms in the Eulerian conservation laws. The numerical implementation of both processes has attracted attention in past studies. The Lagrangian–Eulerian coupling method proposed by Beard et al. (2000), introducing a sphere of momentum influence along the parcel trajectories, seems to improve the phase coupling but on a rather arbitrary physical assumption. A similar idea was employed lately by Sterno et al. (2006), who introduced a gaseous sphere per liquid droplet parcel in order to better represent the mixing of high-speed liquid jets. This approach was found to improve the evaporation and break-up sub-models by controlling the mass exchanged between the two-phases, which effectively delays the addition of spray source terms to the gas phase equations; however, no thorough validation against spray measurements has been presented and in addition the method was not tested for refined grids. The weighting scheme for the distribution of the liquid/gas source terms suggested by Golovitchev and Nordin (2001), based on the reciprocal of the distance between the parcel and the eight nearest nodes (in a hexahedral mesh) raised to an integer power, improves the dependency of predictions on the numerical grid. Furthermore, Lippert et al. (2005) proposed a methodology for momentum coupling that can be applied to meshes of arbitrarily structure, shape and topology, utilising a least-square-based interpolation scheme for gas-to-liquid coupling and a kernel smoothing scheme for liquid-to-gas coupling. Simulations were performed without accounting for break-up, collision and evaporation processes in order to allow for the effect of the momentum coupling between the two phases to become clear. It was concluded that the proposed model was effective, even for coarse meshes, in eliminating grid numerical artefacts on the spray shape; this cannot be guaranteed with the standard method of phase coupling in Eulerian–Lagrangian codes that estimate the gas-to-liquid and the liquid-to-gas transfer only using the cell hosting the dispersed phase parcels. Further complications with grid dependency of Eulerian–Lagrangian calculations have been also realised through modelling of droplet-to-droplet interactions. In particular, Barroso et al. (2003) found that liquid penetration results to be highly dependent on grid-resolution if coalescence is taken into account. Schmidt and Rutland (2000) and Schmidt and Rutland (2003) introduced an algorithm where a second mesh separate from the gas phase grid was employed for the droplet collisions calculation resulting to less grid sensitivity. Since despite the above described efforts, the numerical problems of the Eulerian–Lagrangian methodology have not been overcome, some authors have computed the spray atomisation process near the nozzle using an 1-D approach which provides ad hoc source terms (from mass, momentum and energy exchanges) as input to the multi-dimensional CFD flow solver (Wan and Peters, 1997; Abraham and Magi, 1999). With this approach, the exchange source terms estimated from the 1-D model do not depend on the multi-dimensional mesh resolution; on the other hand, the results of the 1-D model are highly case-dependant and thus, they can be only viewed as a user-adjustable methodology (Versaevel et al., 2000). Recent studies remarked that spray calculations performed for full engine simulation cases show mesh dependence, mainly attributable to the insufficient resolution of the liquid–gas momentum transfer, which is a consequence of the inadequate spatial resolution of the strong velocity and vapour concentration gradients. This is a result of the magnitude of the injection velocity of the liquid phase, typically of hundreds of meters per second, into an almost quiescent environment hereby creating a strong velocity gradient at the nozzle exit. Simulation of liquid phase penetration is sensitive to the size of computational cells, especially for small droplets and increased gas density. If the computational cells are small enough to capture the velocity gradients close to the injector, this will result in the development of a gaseous jet with velocity close to that of the liquid. When the grid is too coarse, numerical diffusion together with lower increase in air velocity results in a much higher relative velocity between the two phases (Golovitchev and Nordin, 2001); inevitably, this affects the outcome of the physical sub-models of droplet break and vaporisation, which depend on the relative velocity between the two phases. Local mesh refinement can be utilised for the resolution of small-scale flow structures near boundaries and in regions of high velocity gradients (Bensler et al., 2000). Establishment of sufficient criteria and integration of fully adaptive mesh refinement into the solution process as function of the phenomena taking place represent fundamental steps for effective dense spray investigations, as discussed by Tristano et al. (2003) and Wan et al. (2003). Finally, Steiner (2004) has recommended that the demand for CFD models for industrial applications, with a high degree of predictability and low computational cost, requires 'intelligent meshing strategies' making crucial the resolution of relevant length-scales with proper coupling and experimental validation between the internal nozzle flow with the subsequent spray development.

Although fuel sprays are usually modelled using a Lagrangian treatment of representative droplet parcels, it is generally recognised that this methodology is suitable for dilute sprays but it has shortcomings with respect to modelling of dense sprays (v. Berg et al., 2001). An alternative approach for simulating dense Diesel sprays has been proposed by v. Berg et al. (2001) and Tomiyama (2002), who implemented a modified two-fluid Eulerian/Eulerian method treating different size classes of the spray droplets as separate and inter-penetrating phases and solving conservation equations for each one of them. The model is based

on an Eulerian multiphase approach that has been derived from ensemble averaging of the conservation equations (Alajbegovic et al., 1999). For each phase, mass, momentum and energy conservation equations are solved as well as corresponding equations for the turbulent kinetic energy and its dissipation rate. Within each computational cell the droplet phases are characterised by a certain volume fraction. The model has been applied to Diesel injection test cases using realistic injection conditions. The effect of inlet conditions, various droplet drag coefficient formulations, droplet aerodynamically-induced secondary break-up, evaporation and collision models have been tested. A disadvantage of this method is that the number of equations to be solved dramatically increases when the droplet size distribution becomes wider and therefore the number of droplet size classes considered increases. Platzer and Sommerfeld (2002) suggested the prediction of the droplet size distribution to be based on maximum entropy formalism. The droplet size distribution, their volume fraction and velocities are eventually used as input conditions to the Lagrangian method which allows a reliable prediction of sprays by accounting for all the relevant physical effects. A different Eulerian–Eulerian methodology has been lately introduced (Beck and Watkins, 2004), where the poly-dispersed nature of the spray is modelled through the use of probability density functions based on the moments of the droplet number size distribution. Transport equations are written for the two moments which represent the liquid mass and surface area, while two more moments representing the mean size and droplet number are approximated via use of a truncated presumed distribution function which is allowed to vary in space and time. More recently, Lebas et al. (2005) and Beau et al. (2005) used a 3-D model for the liquid atomisation process based on an Eulerian single-phase approach, initially proposed by Vallet et al. (2001), which improves the treatment of the interaction between the liquid and the gas phases in the very dense spray region, close to the injector nozzle. This approach considers the liquid and the gas phases as a mixture of a single-fluid with variable density. The method switches to Lagrangian calculations when the spray is considered to be diluted enough based on a dilution criterion, such as a critical value of the liquid volume fraction. This work suggests implementation of a combined hybrid Eulerian–Eulerian and Eulerian–Lagrangian methodology, which represent a promising solution to the discussed numerical issues related to dense-particle multi-phase flow models. It is also worth mentioning that in the majority of the CFD codes applied for spray simulations, irrespectively if the Eulerian–Eulerian or the Eulerian–Lagrangian methodology is employed, the sub-model of atomisation is rather important because it provides the initial estimate of the droplets before other processes become more influential. The atomisation sub-models most widely used are based on the linear instability theory, developed more than 20 years ago by Reitz and Bracco (1982) and later on extended by Huh and Gosman (1991) for liquid turbulence effects to be considered. Additionally, a model to include the presence of cavitation in a rather empirical way has been developed by Arcoumanis and Gavaises (1998). The main limit of all these atomisation models is that they are rather empirical, and thus depend on the specific nozzle geometry used. They effectively predict a mean droplet size, as function of the injection velocity and cavitation vapour volume fraction while the droplet size is then randomly sampled from a pre-defined distribution function; inevitably, empirical tuning of the constants appearing in the model's equation is required. Recently, VOF-based multi-dimensional models have been employed into the modelling of atomisation from'first principles'. The work of Bianchi et al. (2004) has employed a two-dimensional (2-D) volume of fluid (VOF) – large eddy simulation (LES) method to account for the droplet formation at the exit of a single hole nozzle. The 2-D simulation of atomisation, although can be a useful exercise for liquid jets injected from axi-symmetric single-hole nozzles at low Reynolds numbers (i.e. the Rayleigh instability regime), it does not reflect the reality of current injection systems. One of the first examples of three-dimensional (3-D) simulations has been presented by Villiers et al. (2004), who investigated the effect of nozzle flow conditions on liquid jet atomisation using 3-D VOF-LES simulation. The grid size used in that study was 10 μm in the atomisation region. As a result, the minimum droplet size that could be predicted was ~50 μm, which is far from the size of the droplets of automotive sprays. Bianchi et al. (2005) performed similar 3-D VOF-LES simulations of the liquid jet atomisation using smaller cell sizes of 8 μm and in a more recent study, Bianchi et al. (2007), the minimum cell size has been reduced down to 4 μm. The numerical code used employs however structured meshes, which is the main reason for not being able to use finer grids able to resolve smaller structures near the atomisation region. Furthermore, the liquid was exiting from a single-hole axi-symmetric and cavitation-free nozzle. The study, although in the right direction for resolving the flow development in the near nozzle exit, is still far from representing the actual flow conditions of automotive injectors while the simulation time required is of the order of weeks for parallel computations.

The present paper describes and assesses against experimental data an Eulerian–Lagrangian numerical methodology for dense spray simulations. The originality of the numerical methodology proposed here consists of the simultaneous employment of three steps, namely (i) distribution of the source terms expressing the mass, momentum and energy coupling between the two phases into a number of arbitrarily shaped grid cells found in the vicinity of the droplet, (ii) estimation of the air flow properties at the time scale of droplet movement through introduction of so-called 'virtual properties' which prevent from non-physical values for the exchange source terms to be calculated and (iii) application of adaptive local grid refinement in the area of liquid injection, which gives the desired grid resolution without compromising in computational time. The model can be easily implemented in existing CFD codes without

the need to switch to Eulerian–Eulerian calculations while at the same time can result to grid-independent solution for refined grids. The various phenomenological sub-models required for prediction of the sub-grid time and scale processes have been also thoroughly investigated and the corresponding results are presented in Tonini (2006). In the next paragraphs the numerical model is presented, followed by a description of the test cases used for model validation. The numerous test cases simulated are then presented; 2-D cases have allowed assessment of the model at reduced computational time while 3-D cases demonstrate the applicability of the model to realistic configurations. Results from numerous parametric studies are also presented. In addition to the effect of the parameters involved in the three aforementioned numerical methods, further test cases assess and quantify against experimental data the influence of a number of parameters involved in the simulation model, including the discretisation scheme of the governing equation simulating the air motion, the time step used to resolve the air and spray development and the number of computational parcels comprising the fuel plume. Validation of the model is performed with comparison against experimental data for the liquid and vapour penetration of a Diesel spray injected with pressure up to 1200 bar against pressurised air.

## 2. Model description

The simulation of the continuous phase, which describes the gas motion during the spray injection is performed using the GFS (General Fluid Solver) code, developed by the authors within their research group. This is a 3-D, transient, turbulent and multi-phase flow solver that can be applied to geometries with moving boundaries. A brief mathematical formulation of the governing flow equations considered is given below for purposes of completeness while emphasis is placed on the numerical methodology developed for coupling the interaction of the liquid and gaseous phases during the development of liquid sprays.

### 2.1. Continuous phase equations

The time-averaged form of the incompressible Navier–Stokes equations describing the continuity, momentum and conservation equations for any scalar variables is expressed as follows:

$$\begin{aligned}
&\frac{\partial}{\partial t}(\alpha_C\rho_C) + \nabla\cdot(\alpha_C\rho_C\mathbf{u}) = \mathbf{s}_m \\
&\frac{\partial}{\partial t}(\alpha_C\rho_C\mathbf{u}) + \nabla\cdot(\alpha_C\rho_C\mathbf{u}\otimes\mathbf{u} - \alpha_C\mathbf{T}) = \mathbf{s}_\mathbf{u} \\
&\frac{\partial}{\partial t}(\alpha_C\rho_C\varphi) + \nabla\cdot(\alpha_C\rho_C\varphi\mathbf{u} - \alpha_C\mathbf{q}) = \mathbf{s}_\varphi \\
&\alpha_C = 1.\left(-\frac{V_{P,C}}{V_C}\right)
\end{aligned} \tag{1}$$

here $\rho_C$ is the continuous-phase density in the cell with volume $V_C$, $V_{P,C}$ the total volume of the dispersed phase in the cell, $\alpha_C$ its void volume fraction, $\varphi$ any scalar variable (i.e. temperature, concentration, turbulent kinetic energy), $\mathbf{q}$ its flux vector, $\mathbf{u}$ the velocity vector and $\mathbf{T}$ the stress tensor defined as:

$$\mathbf{T} = -\left(P + \frac{2}{3}\mu_C\nabla\cdot\mathbf{u}\right)\mathbf{I} + \mu_C[\nabla\otimes\mathbf{u} + (\nabla\otimes\mathbf{u})^T] \tag{2}$$

where $\mathbf{I}$ is the unit tensor, $\mu_C$ the continuous phase dynamic viscosity and $P$ the static pressure. For the generic scalar variable $\varphi$ the diffusion flux vector $\mathbf{q}$ is calculated as

$$\mathbf{q} = \Gamma\nabla\varphi \tag{3}$$

where $\Gamma$ is the diffusion factor:

$$\Gamma = \frac{\mu_C}{Pr} \tag{4}$$

$Pr$ is the Prandtl number for the scalar variable $\varphi$. The source terms on the right-hand side of the above equations are due to mass, momentum and energy exchange between the two phases. The effect of turbulence on the fluid flow is predicted by the standard $k-\varepsilon$ model of Launder and Spalding (1972). The GFS code implements an iterative algorithm, using a combination of solvers from the extensive SLAP library to solve the transport equations, on collocated curvilinear non-orthogonal computational grids. The numerical simulation of the basic conservation equations in based on the finite volume method for incompressible flows using a pressure correction method (Caretto et al., 1972; Rhie and Chow, 1983; Issa, 1986) and appropriate boundary conditions. The convection term, in the general form of the conservation equation for the generic flow quantity $\varphi$, can be discretised using different differencing schemes. Here, the effect of three schemes, named 'Hybrid', 'NVD' (Jasak et al., 1999) and 'BSOU' (Papadakis and Bergeles, 1995) have been implemented. As far as the temporal discretisation of the term representing the rate of change per unit volume of the generic flow quantity $\varphi$, the explicit Euler as well as the fully implicit and unconditionally stable Crank–Nicolson schemes have been tested.

### 2.2. Dispersed phase equations

The Lagrangian formulation is based on the fluid-particle model introduced by Dukowicz (1980). The model assumes that the inter-phase transport of mass, momentum and energy is quasi-steady and their transfer coefficients to/and from the droplets are independent from the proximity of neighbouring droplets and can be represented by empirical correlations. Within the context of the Lagrangian framework, it is necessary to simulate the large number of particles by means of a stochastic statistical approximation (of the order of 10,000–100,000 during a typical injection event). With this approximation the total droplet population is represented by a number of parcels, each containing a large number of identical and non-interacting

droplets. The properties of these representative parcels are randomly approximated from empirical or calculated distribution functions, using a Monte-Carlo approximation. In order to describe statistically the total droplet population, a distribution function $f(\mathbf{x}, \mathbf{u}, R, T, t)$ is assumed, which determines at time $t$ the probable number of droplets per unit volume that is located in the spatial range ($\mathbf{x}$, $\mathbf{x}+\partial\mathbf{x}$), with velocity in the range ( $\mathbf{u}$, $\mathbf{u}+\partial\mathbf{u}$), radius in the range ($R$, $R+\partial R$) and temperature in the range ($T$, $T+\partial T$). For the conservation of the total number of droplets in any volume of ($\mathbf{x}$, $\mathbf{u}$, $R$, $T$, $t$), the following Liouville equation must be satisfied:

$$\frac{\partial f}{\partial t}+\nabla_{\mathbf{x}}(f\cdot\mathbf{u})+\nabla_{\mathbf{u}}\left(f\cdot\frac{\mathrm{d}\mathbf{u}}{\mathrm{d}t}\right)\frac{\partial}{\partial T}\left(f\cdot\frac{\mathrm{d}T}{\mathrm{d}t}\right)+\frac{\partial}{\partial m}\left(f\cdot\frac{\mathrm{d}m}{\mathrm{d}t}\right)=\dot{f}_{\mathrm{inj}}+\dot{f}_{\mathrm{atom}}+\dot{f}_{\mathrm{break}}+\dot{f}_{\mathrm{coll}}+\dot{f}_{\mathrm{turb}} \quad (5)$$

where the various terms at the r.h.s. (right hand side) of this equation represent the temporal variations in the liquid droplet size distribution function due to fuel injection, liquid core disintegration, droplet secondary break-up, droplet collision and coalescence and liquid–gas turbulence dispersion, respectively. In order to solve the above equation, the Lagrangian approximation method has been utilised. All the physical processes referred to as source terms in Eq. (5) are calculated through corresponding sub-models. Within the context of the aforementioned method, the continuum distribution function $f$ is approximated with a discrete number of computational parcels; this approximation for function $f$ reads in equation form as follows:

$$f(\mathbf{x},\mathbf{u},R,T,t)=\sum_{\mathrm{P}}N_{\mathrm{pP}}\delta(\mathbf{x}-\mathbf{x}_{\mathrm{P}})\delta(\mathbf{u}-\mathbf{u}_{\mathrm{P}})\delta(R-R_{\mathrm{P}})\delta(T-T_{\mathrm{P}}) \quad (6)$$

where $N_{\mathrm{pP}}$ is the number of identical particles represented by parcel P. This number is defined when a new parcel is injected; obviously, the total number of parcels has to be high enough to yield statistical independence of the predicted results.

The physical sub-models used for estimating the above source terms and solving Eq. (5) are thoroughly investigated in Tonini (2006). Here, only a brief description is given for purposes of completeness. The droplet initial properties are determined by the flow conditions at the exit of the injector nozzle. This provides estimates for the transient flow rate, injection velocity and droplet size, as shown by Arcoumanis et al. (1997). The liquid-core fragmentation process at the exit of hole-type injectors is simulated by the so-called turbulence-induced (Huh and Gosman, 1991) and cavitation-induced atomisation models (Arcoumanis and Gavaises, 1998). Droplet drag coefficient, which determines to a large extent the momentum exchange between the gas and the liquid phases, is modelled considering the effect of droplet movement in an evaporating environment, presence of other droplets, internal flow circulation and non-spherical droplet shape (Feng and Michaelides, 2001). Effects such as multi-component fuel vaporisation, internal liquid circulation, temperature variation within the droplet, diffusion between the different fuel compounds, gas solubility as well as droplet deformation and departure from ideal behaviour in the phase equilibrium relationship are also considered (Aggarwal and Mongia, 2002; Hohmann and Renz, 2003; Trujillo et al., 2004; Sazhin, 2006). Droplet aerodynamic break-up plays an important role on the predictions of the droplet size population. The model used combines correlations from various literature findings in order to predict the mean droplet diameter, droplet deformation and droplet break-up time over a wide range of Weber numbers (Arcoumanis et al., 1997). Then, the droplet size is randomly sampled from a distribution function, which is calculated using the maximum entropy formalism. Finally, droplet turbulent dispersion is modelled according to O'Rourke (1989), while droplet collisions and coalescence are modelled using a modified version of the model of O'Rourke (1981); according to Gavaises et al. (1996) the probability of collisions between droplets is not calculated for droplet parcels contained on the same cell but rather for droplets found within a distance proportional to the parcel size.

### 2.3. Solution procedure

Regarding the solution procedure algorithm, the dispersed phase part is calculated initially; due to the different time scales inherent to the development of two phases the selected tracking time step for the dispersed phase $\Delta t_{\mathrm{P}}$ is much smaller than the corresponding one $\Delta t_{\mathrm{C}}$ for the continuous gaseous phase. This is according to the Courant number restriction:

$$CN=\frac{|\mathbf{u}_{\mathrm{P}}|\Delta t_{\mathrm{P}}}{\Delta l}\leqslant CN_{\max}<1 \quad (7)$$

where $CN$ and $CN_{\max}$ are the cell and the maximum allowed Courant numbers, typically in the range of 0.1–0.3, $\Delta l$ is a typical cell length, which is characteristic of the control volume of the parcel location. The parcel tracking time step should be smaller than the residence time of the parcel in the computational cell (i.e. the time interval spent by the parcel to travel through the selected cell), in order to guarantee the correct interpolation/distribution of the multiphase coupling. Consequently, finer grids require smaller time steps. This is particularly important in case of dynamically refined grids, which require introduction of variable time steps. As a consequence, a number of sub-cycles need to be performed within the dispersed phase part, enough to reach the time-level of the continuous phase, and subsequently the continuous phase part is calculated. The basic computational steps in the droplet phase part can be summarised as follows:

1. Liquid injection and atomisation.
2. Calculation of newly formed droplet location due to initial velocity.

3. Interpolation of scalar and vector quantities from continuous air phase solution at the new location of the droplet parcels.
4. Computation of droplet aerodynamic drag, break-up, vaporisation, turbulence dispersion,collisions and coalescence.
5. Estimation of void-fraction due to the presence of the droplets; calculation of mass,momentum and energy interaction source terms for the continuous phase.

Some steps in the above synopsis need to be explained in detail, since they posed a great challenge during the development of the current model, from a numerical point of view.

### 2.4. Droplet volume-fraction calculation

Generally speaking, the coupling of the Eulerian continuous gaseous phase with the Lagrangian dispersed droplet phase can become problematic when some inherent assumptions of the methodology tend to be violated. The most important assumptions of all Eulerian–Lagrangian methodologies is that the dispersed phase volume fraction remains relatively low, and that the typical dimensions of the parcels under consideration remain much smaller than the typical cell size of the Eulerian mesh. These assumptions can be violated in dense liquid droplet flows, if dense grids are used. One should note that the violation of the second assumption can take place not only for an Eulerian–Lagrangian droplet-based model, but also for an Eulerian–Eulerian one; this poses a theoretical weakness for this approach as well. In order to circumvent this limitation, a numerical methodology was developed, with which the excess volume of each droplet parcel could be distributed to its surrounding Eulerian cells. Normally, for the calculation of the volume fraction of a single droplet parcel with volume smaller than that of its host cell $V_C$ the following expression would suffice:

$$\alpha_P = \frac{1}{\Delta t V_C} \int_t^{t+\Delta t} \frac{4}{3} \pi R_P^3 N_P \Delta t \tag{8}$$

With the above equation the time-averaged dispersed phase volume fraction would be calculated for each cell, provided that the total volume of the droplet parcels present in this cell would be smaller than the volume of the cell itself at all times. Time-averaging is necessary, due to the fact that the time step for the solution of each dispersed phase sub-cycle can be much smaller than the time step for the continuous phase solution, and so it is possible that parcels convey through a number of cells during the 'sub-cycling' part of the solution procedure. In order to account for this, during each dispersed phase sub-cycle the volume fraction of the droplets is calculated for each cell, subsequently it is multiplied by the dispersed/continuous phase time step ratio, namely $\Delta t_P/\Delta t_C$, and then it is summed over all the dispersed phase time steps. In order to establish a conservative approach and to address this problem a special methodology was devised; droplets can be larger than the cell they are occupying, and then the excess volume of the host cell is distributed to its adjacent ones. If any of the adjacent cells is already full of liquid, the distribution continues to cells that are located further, until the excess volume is consumed. It should be stressed that this approach must be considered as an approximate solution to the problem; in no way can this method substitute the much more accurate interface capturing and tracking techniques, which are used for direct simulation of droplet motion. Once the distribution of the excess droplet volume is completed for all parcels, the volume fraction of the dispersed phase is calculated using the following equation, which is a reformulation of Eq. (8):

$$\alpha_P = \frac{1}{\Delta t_C V_C} \int_t^{t+\Delta t} V_{P,C} \Delta t_P \tag{9}$$

where obviously $V_{P,C}$ is the volume of dispersed phase in the cell. From the dispersed phase volume fraction the continuous phase void fraction is obviously calculated from the following equation:

$$\alpha_C = 1 - \alpha_P \tag{10}$$

### 2.5. Two-phase coupling

Here, the methodology adopted for estimating the flow variables 'seen' by the discrete droplet parcels as they move in the surrounding fluid and the estimation of the source terms expressing the mass, momentum and energy exchanged between the liquid and the gaseous phases is described. A combination of different interpolation/distribution methods can be generally employed; some possible options are summarised and their effect on model predictions is assessed. Within the context of the 'standard' Lagrangian methodology, the values of the continuous phase properties (temperature, pressure, velocity, density, viscosity, heat capacity, turbulence and liquid volume fraction) at the parcel location are set equal to those of the cell containing parcel; this can be mathematically expressed by the following equation:

$$\varphi(\mathbf{x} = \mathbf{x}_P) = \varphi(\mathbf{x} = \mathbf{x}_C) \tag{11}$$

where $\varphi$ is the requested scalar/vector quantity at the parcel location, and $\mathbf{x}_P$ and $\mathbf{x}_C$ are the locations of the parcel centre and host cell centre, respectively. As mentioned, application of this algorithm to the simulation of high-pressure dense Diesel sprays is sensitive to the grid size. A demonstration of that can be realised in Fig. 1, which shows the development of a liquid fuel spray injected into a quiescent air of 30bar and 800 K; the simulations have been performed on grids with spacing between 2 mm down to 0.5 mm. The images present the spray development at 0.6 ms after start of injection (ASOI); the initial size of the liquid droplets follows a pre-defined distribution function with Sauter mean diameter (SMD) equal to 15 μm.

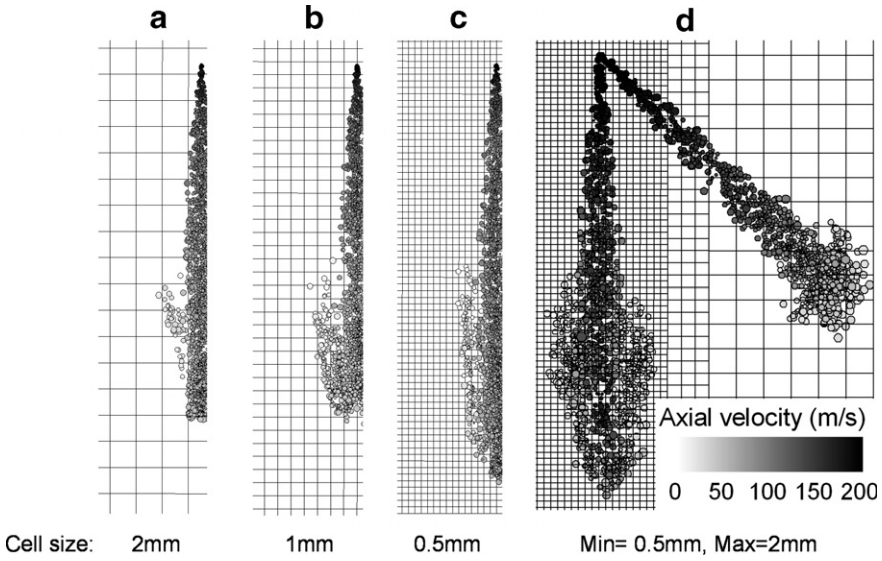


Fig. 1. Effect of grid cell size on predicted spray structure at 0.6 ms ASOI using: (a) 2 mm uniform grid, (b) 1 mm uniform grid (c) 0.5 mm uniform grid and (d) grid with variable cell size between 0.5–2 mm; source terms are given to the cell-containing parcel; case 1 of Table 1.

Case 1 of Table 1 summaries the injection conditions used as input for these simulations. In order to isolate the computational domain effect from the physical processes taking place during the spray development, the liquid core atomisation, droplet secondary break-up, coalescence, turbulent dispersion and evaporation models have been deactivated. Fig. 1a–c show the remarkable effect of the grid spatial resolution on the spray structure: the spray penetration significantly increases as the grid is refined. Fig. 1d shows the spray development under the same operating conditions, using a non-uniform computational grid. Now, two different cases have been simulated using identical injection conditions; the first spray penetrates in the homogeneous fine region, while in the second case the spray develops from the finer towards the coarser grid region. The spray shape, which should have been identical in these two cases, is considerably influenced by the grid density, due to the non-homogeneous grid cell density. It ought to be mentioned that this method does not allow infinite grid refinement, since the flow solver solution will diverge using more refined grids due to the incorrect estimation of the momentum source term.

An improved interpolation method can be based on the assumption that the region of influence between the two phases should be independent on the cell size, but should be rather based on a predefined distance $r$, which can be equal to a fixed constant value or even function of an equivalent parcel size. The cells found within this distance are initially identified; the numerical method implemented can consider any type of cells, i.e. tetrahedrons, hexahedrons, pyramids and prisms used here, which makes it applicable to complex 3-D geometries. A weighting factor, $\delta_i$ function of this distance, rather than the cell volume, is used for the interpolation of the continuous phase variable, according to the following equation:

$$\varphi(\mathbf{x}=\mathbf{x}_{\mathrm{P}})=\sum_{i=1}^{N_{\mathrm{C}}}\varphi(\mathbf{x}=\mathbf{x}_{\mathrm{C}_i})\delta_i \tag{12}$$

where the weighting factor $\delta_i$ is expressed as follows:

$$\delta_i=\frac{\lambda_{\mathrm{C}_i}/(\gamma \mathrm{dist}_i/r+1)}{\sum_{i=1}^{N_{\mathrm{C}}}\lambda_{\mathrm{C}_i}/(\gamma \mathrm{dist}_i/r+1)},\quad i=1,N_{\mathrm{C}} \tag{13}$$

$\lambda_{\mathrm{C}_i}$ represents either a proportionality factor or the cell volume, $\gamma$ is a user-defined constant increasing the relative weight of the closer cells and $N_{\mathrm{C}}$ is the total number of cells found within this region. The parcel-to-cell relative distance is defined as

$$\mathrm{dist}_i=|\mathbf{x}_{\mathrm{C}_i}-\mathbf{x}_{\mathrm{P}}| \tag{14}$$

The coupling between the gas and the liquid phases is expressed through appropriate source terms which express the mass, momentum and energy multi-phase exchange in the fluid flow conservation equations. These are mathematically correlated with the Lagrangian approximation of the spray distribution function, $f(\mathbf{x}, \mathbf{u}, m, T, t)$ as follows. The mass source term resulting from the droplet evaporation process is defined by the following expression:

Table 1
Operating conditions for the four cases investigated, cases 2, 3 and 4 correspond to the experimental data base of König and Blessing (2003)

| Case | 1 | 2 | 3 | 4 |
|---|---|---|---|---|
| Injection flow rate ($mm^3/ms$) | 7.5 | 6 | 15 | 15 |
| Injection pressure (bar) | 500 | 300 | 1200 | 1200 |
| $T_{back}$ (K) | 800 | 273 | 273 | 900 |
| $P_{back}$ (bar) | 30 | 20 | 20 | 54 |
| Fuel | $n$-$C_{12}H_{26}$ | $n$-$C_{13}H_{28}$ | $n$-$C_{13}H_{28}$ | $n$-$C_{13}H_{28}$ |

$$\mathbf{s}_{m,k} = \int f(\mathbf{x},\mathbf{u},m,T,t)\frac{\mathrm{d}m_k}{\mathrm{d}t}\mathrm{d}\mathbf{x}\,\mathrm{d}\mathbf{u}\,\mathrm{d}m_k\,\mathrm{d}T \tag{15}$$

where $\frac{\mathrm{d}m_k}{\mathrm{d}t}$ represents the liquid vaporisation rate for each species $k$ in the liquid composition. The momentum exchange between the two phases is due to the relative velocity and droplet mass changes, as a consequence of the forces exerting upon the moving droplets and the evaporation process, respectively; this is expressed as

$$\mathbf{s}_{\mathbf{u}} = \int f(\mathbf{x},\mathbf{u},m,T,t)\left[m\frac{\mathrm{d}\mathbf{u}}{\mathrm{d}t} + \mathbf{u}\frac{\mathrm{d}m}{\mathrm{d}t}\right]\mathrm{d}\mathbf{x}\,\mathrm{d}\mathbf{u}\,\mathrm{d}m\,\mathrm{d}T \tag{16}$$

Finally the energy coupling term takes into account the heat flux between the two phases and the kinetic energy variations, due to the acceleration or deceleration of the parcel flowing in the continuum surrounding:

$$\mathbf{s}_{\varphi} = \int f(\mathbf{x},\mathbf{u},m,T)\left[\frac{\mathrm{d}m}{\mathrm{d}t}\left(\frac{\mathbf{u}^2}{2} + C_{\mathrm{P}_l}T\right) + m\left(\left|\mathbf{u}\frac{\mathrm{d}\mathbf{u}}{\mathrm{d}t}\right| + C_{\mathrm{P}_l}\frac{\mathrm{d}T}{\mathrm{d}t}\right)\right]\mathrm{d}\mathbf{x}\,\mathrm{d}\mathbf{u}\,\mathrm{d}m\,\mathrm{d}T \tag{17}$$

The above source terms are estimated during the sub-cycles of the discrete phase and they are then added explicitly to the right hand side of the continuous phase conservation equations.

Within the context of the standard Lagrangian methodology, the source terms are added to the cell-containing parcel. Alternatively, the source terms can be distributed among the cells of the computational domain, in a way similar to that described above for the interpolation of the continuous phase variables to the parcel location (Eqs. (12)–(14)). The total source term exchanged by the parcel $P$ with its surrounding, calculated from Eqs. (15)–(17),is distributed among the cells found in the region of influence:

$$\mathbf{s}_i = \mathbf{s}\delta_i, \quad i = 1, N_{\mathrm{C}} \tag{18}$$

where $\mathbf{s}_i$ represents the contribution of the source term to the cell $i$ and $\delta_i$ the weighting factor.

The weighting factor is a function of the parcel-to-cell distance, cell volume and cell internal energy. The cell volume contribution to the weighting factor is expressed through the relation:

$$\delta_i = \frac{V_{\mathrm{C}_i}}{\sum_{i=1}^{N_{\mathrm{C}}} V_{\mathrm{C}_i}}, \; i = 1, N_{\mathrm{C}} \tag{19}$$

where $V_{C_i}$ represents the volume of the cell $i$. Another spatial distribution approach can be based on the distance between the parcel and the cells in the region of influence, with closest cells giving a bigger contribution, as expressed by the following equation:

$$\delta_i = \frac{1/(\gamma \mathrm{dist}_i/r + 1)}{\sum_{i=1}^{N_{\mathrm{C}}} 1/(\gamma \mathrm{dist}_i/r + 1)}, \quad i = 1, N_{\mathrm{C}} \tag{20}$$

where dist, $r$ and $\gamma$ correspond to the distribution variables defined in Eq. (13). In order to consider the effect that the source terms should be exchanged during the time step of the Lagrangian motion of the parcels and not just at the beginning and ending points of their displacement, the final parcel location, $\mathbf{x}_{\mathrm{p}}$, can be replaced by an average point corresponding to the middle distance travelled by the droplet parcel during its tracking time:

$$\mathbf{x}_{\mathrm{P}} = 0.5(\mathbf{x}_{\mathrm{P}}^{\mathrm{old}} + \mathbf{x}_{\mathrm{P}}^{\mathrm{new}}) \tag{21}$$

where $\mathbf{x}_{\mathrm{P}}^{\mathrm{old}}$ and $\mathbf{x}_{P}^{\mathrm{new}}$ represent the parcel location at start and at the end of the dispersed phase time step, respectively. In this case the predefined distance $r$ is taken equal to the distance covered by the droplet parcel:

$$r = 0.5\sqrt{(\mathbf{x}_{\mathrm{P}}^{\mathrm{new}} - \mathbf{x}_{\mathrm{P}}^{\mathrm{old}}) \cdot (\mathbf{x}_{\mathrm{P}}^{\mathrm{new}} - \mathbf{x}_{\mathrm{P}}^{\mathrm{old}})} \tag{22}$$

The third distribution method results from the combination of the cell volume and the distance of each cell from the parcel location:

$$\delta_i = \frac{V_{\mathrm{C}_i}/(\gamma \mathrm{dist}_i/r + 1)}{\sum_{i=1}^{N_{\mathrm{C}}} V_{\mathrm{C}_i}/(\gamma \mathrm{dist}_i/r + 1)}, \quad i = 1, N_{\mathrm{C}} \tag{23}$$

Finally, a distribution method taking into account the internal energy of the cells inside the interaction region between the parcel and the surroundings is defined according to following expression:

$$\delta_i = \frac{V_{\mathrm{C}_i}\rho_{\mathrm{C}_i}C_{\mathrm{PC}_i}T_{\mathrm{C}_i}/(\gamma \mathrm{dist}_i/r + 1)}{\sum_{i=1}^{N_{\mathrm{C}}} V_{\mathrm{C}_i}\rho_{\mathrm{C}_i}C_{\mathrm{PC}_i}T_{\mathrm{C}_i}/(\gamma \mathrm{dist}_i/r + 1)}, \quad i = 1, N_{\mathrm{C}} \tag{24}$$

This method has been proven useful in case of distribution of mass and energy source terms due to liquid droplet vaporisation, since the gas phase internal energy available may represent the limiting factor governing the interaction between the two phases. Fig. 2 shows the sensitivity of the computational results on the source term distribution method. Sample droplets are plotted on a plane perpendicular to the injection direction located 15 mm from the injection point; results are presented from the non-distribution case as well as from a case where the momentum source term is distributed in a number of computational cells for case 1 of Table 1. In this case only the momentum exchanged between the two phases has been simulated, while the effect of break-up, collision/coalescence, vaporisation has not been taken into account. In the first case, the spray splits in four parts, due to the fact that it takes longer time for a droplet to travel through a cell in a direction along the cell diagonal relative to the horizontal and vertical directions; that numerically results in the non-physical picture of Fig. 2a. On the other hand, when the source terms are distributed according to Eq. (23), then a more realistic distribution of the liquid droplets on that plane is obtained, as shown in Fig. 2b; the different distribution methods mentioned result in similar predictions.

The effect of different interpolation/distribution distances on the temporal profiles of liquid and vapour penetrations are also presented for a non-evaporating and an evaporating spray injected with nominal rail pressure of 1200 bar (cases 3 and 4 of Table 1, respectively), taking into account atomisation, aerodynamic drag, break-up,

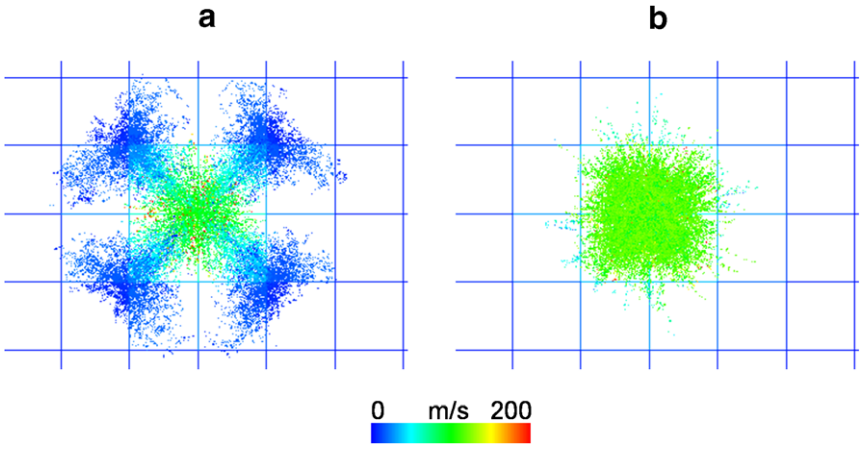


Fig. 2. Effect of source term distribution on calculated spray structure on a plane perpendicular to the injection axis at 15 mm from the injection hole, at 0.6 ms ASOI; (a) source term given to the cell-containing parcel and (b) source term distributed within a region of 0.4 mm from the parcel centre; case 1 of Table 1.

collisions/coalescence, turbulent dispersion and vaporisation processes. The 2-D grid used consists of triangles with minimum resolution near the nozzle exit of approximately 0.30 mm. Results are shown in Fig. 3 using two interpolation/distribution distances, $r$; the first one is equal to a constant value of 0.4 mm and the second one is proportional to the 'equivalent' parcel diameter, estimated from the following correlation:

$$R_{\text{interp/distr,P}} = \gamma D_{\text{P}} = \gamma \sqrt[3]{N_{\text{p,P}} \left(\frac{D_{\text{p,P}}}{2}\right)^3} \tag{25}$$

where $R_{\text{interp/distr,P}}$ represents the interpolation/distribution distance for the parcel P, $\gamma$ is a constant selected equal to 2 and $D_{\text{p,P}}$ stands for the diameter of the particle p in the parcel P, which contains a number equal to $N_{\text{P,p}}$ of identical particles. The sensitivity of the predicted liquid and vapour penetration on the calculated variable $R_{\text{interp/distr}}$ seems to be negligible for non-evaporating sprays, according to Fig. 3a, while it seems to affect the liquid penetration under evaporating conditions, as shown in Fig. 3b. The use of an interpolation/distribution distance proportional to the'equivalent' parcel size slightly over-predicts the experimental liquid penetration, although the percentage standard deviation of the predicted results from the corresponding experimental data is below 5.5%, which represents an acceptable tolerance for the model accuracy. In particular, the sensitivity of the liquid and vapour penetration on the choice of the constant of proportionality $\gamma$ in Eq. (25), which controls the region of influence surrounding the parcel, is shown in Fig. 4. The value of $\gamma$ has been varied from 1 up to 4, which means that the radius of the region of influence for each parcel increases from one up to four times the radius of the computational parcel. The results reveal that this parameter seems not to affect the solution significantly.

### 2.6. Virtual properties estimation

As already mentioned, within the present numerical implementation, the time step used for the simulation of

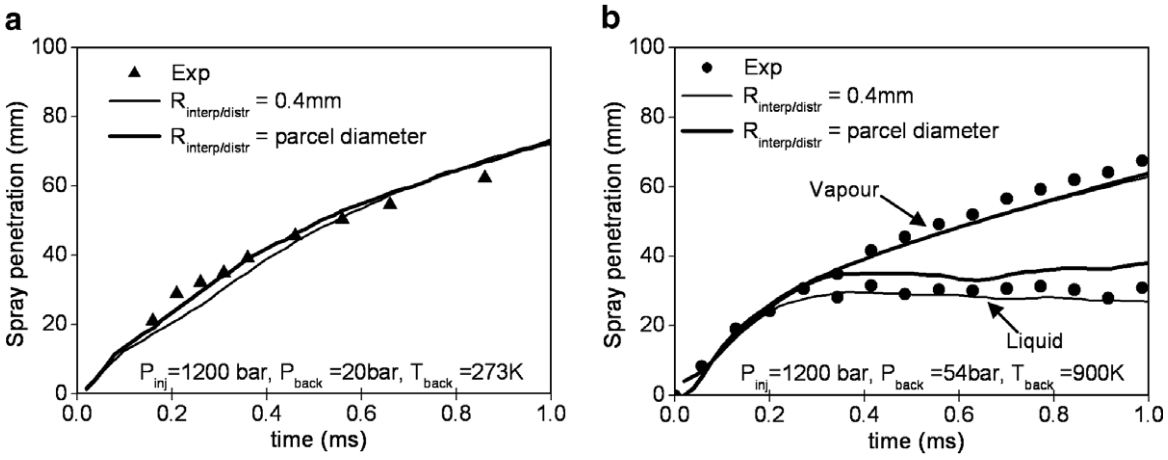


Fig. 3. Effect of interpolation/distribution distance on temporal variation of liquid and vapour spray penetration of non-evaporating and evaporating spray (a) case 3 and (b) case 4 of Table 1.

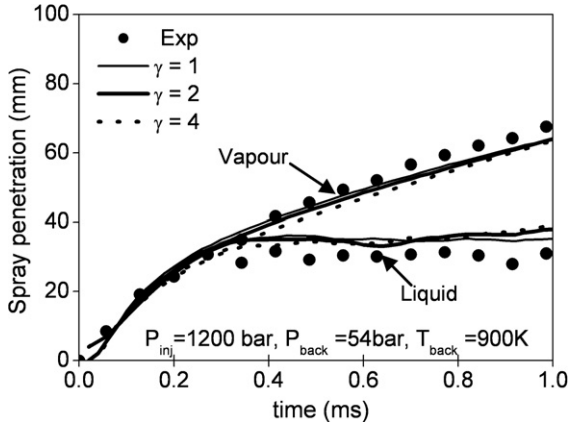


Fig. 4. Effect of constant factor $\gamma$ of Eq. (25) on temporal variation of liquid and vapour penetration for the evaporating spray; case 4 of Table 1.

the gaseous phase motion is approximately two orders of magnitude greater than that of the liquid droplet tracking time step. During that time, a large number of droplets may cross a specific computational cell, exchanging mass, momentum and energy. This necessitates calculations of updated flow variables considering the presence of droplets passing previously from that cell in between successive Eulerian phase time steps. These variables will be referred to here as 'cell-virtual' values for velocity, temperature, species concentration and liquid volume fraction, since they are not a result of the numerical solution of the governing flow equations, but rather estimates obtained in between successive solutions; they are calculated according to the following expression:

$$\phi_{\mathrm{C}}^{\mathrm{new}} = \phi_{\mathrm{C}}^{\mathrm{old}} + \frac{\mathbf{s}_{\mathrm{C}}}{\Psi_{\mathrm{C}}}\Delta t_{\mathrm{P}} \tag{26}$$

where $\phi_{\mathrm{C}}$ represents the value of the 'virtual' cell variable to be estimated, $\mathbf{s}_{\mathrm{C}}$ the generic source term from mass, momentum, energy and volume exchanged between the discrete and the continuous phases, within the tracking time step $\Delta t_{\mathrm{p}}$, and $\Psi_{\mathrm{C}}$ a parameter representing the cell mass or the product between the cell mass and heat capacity at constant pressure. In particular for the calculation of 'virtual' cell velocity, Eq. (26) reduces to:

$$\mathbf{u}_{\mathrm{C}}^{\mathrm{new}} = \mathbf{u}_{\mathrm{C}}^{\mathrm{old}} + \frac{\mathbf{s}_{\mathrm{C}}}{m_{\mathrm{C}}}\Delta t_{\mathrm{P}} \tag{27}$$

where $\mathbf{s}_{\mathrm{C}}$ represents the momentum source term calculated by Eq. (16) and added to the continuous phase using the distribution method of Eq. (19). The physical constraint for updating the value of Eq. (27) is based on the fact that in case of droplet deceleration caused by aerodynamic drag, the velocity of the accelerating air cannot become higher than that of the faster moving droplet, and vice-versa. This has an effect on the momentum exchanged between droplet parcels travelling on the wake of those downstream, or even on the same parcel if its residence time in the same cell is longer than the tracking time step. This constraint plays a significant role particularly in the dense spray region near the exit of the injector hole, where the number of particles and the liquid/gas relative velocities are considerably high and may lead to air velocity values similar to those of the injected fuel. Similarly, the 'virtual' cell species concentrations are estimated according to the following expression:

$$\phi_{\mathrm{C},k}^{\mathrm{new}} = \phi_{\mathrm{C},k}^{\mathrm{old}} + \frac{\mathbf{s}_{\mathrm{C},k}}{m_{\mathrm{C}}}\Delta t_{\mathrm{P}} \tag{28}$$

where the maximum value is obviously 1. Again, this constraint limits the vaporisation process, since the vapour mass fraction surrounding the liquid droplet controls the evaporation mass transfer (Tonini, 2006). Finally the 'virtual' cell temperature is calculated as follows:

$$T_{\mathrm{C}}^{\mathrm{new}} = T_{\mathrm{C}}^{\mathrm{old}} + \frac{\mathbf{s}_{\mathrm{C}}}{m_{\mathrm{C}}C_{\mathrm{PC}}}\Delta t_{\mathrm{P}} \tag{29}$$

In this case, the value is constrained by the internal energy available inside the cell. The physical criterion behind this method is based on the assumption that the surrounding gas cannot become colder than the parcel within the evaporation sub-cycle, if the energy is transferred from the gas to the liquid. In this case the 'virtual' cell temperature is numerically limited to take the parcel temperature value.

Several tests, not shown here, have been performed for investigating the effect of cell 'virtual' properties calculation over a variety of physical and geometrical operating conditions, using different 2-D and 3-D computational domains with variable cell size and implementing the interpolation and source term distribution methods described. Generally, the results suggest that the estimation of cell 'virtual' properties have an effect in limiting the source terms calculated during the parcel sub-cycles, and preventing the continuous phase variables to take non-physical values, particularly in case of dense sprays developing in fine computational domains. An example can be seen in Fig. 5, where the temporal variation of the air velocity and temperature 'seen' by one parcel are plotted; predictions refer to three simulations performed with and without the contribution of the 'cell virtual' properties for the case 4 of Table 1; these are indicated as cases 1/a, 1/b and 1/c in Table 3. The calculation of cell virtual properties has been considered only for case 1/a where the time step for the solution of the flow field variables is equal to $10^{-5}$ s. The same value has been used for case 1/b, but without estimating cell virtual values, while it has been decreased down to $5 \times 10^{-7}$ s for case 1/c. This is the same as the tracking time step used for the liquid droplet parcels; that has been kept fixed for the three cases considered. The results obtained without considering the 'cell virtual' properties and using the long time step for the continuous phase (case 1/b) take non-physical values at 0.01 ms after start of injection and both the flow field velocity and gas temperature solutions diverge. On the other hand, estimation of the 'cell virtual' properties, which limit the source terms exchanged between the two phases, guarantees realistic results. In this case the

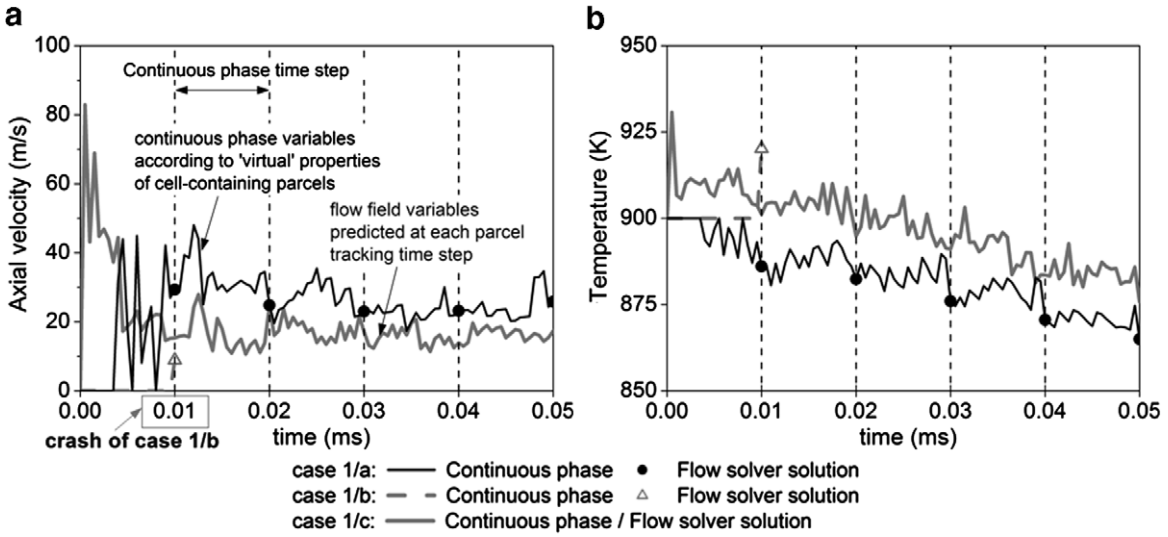


Fig. 5. Effect of 'cell-virtual' velocity calculation on the prediction of the continuous phase and mean flow field (a) axial velocity and (b) temperature; the source terms are given to the cell-containing parcel; Case 1/a,b,c of Table 3.

Table 2
Description of the computational grids used

| Grid | Min cell size (mm) | Max cell number | Cell type | Description |
|---|---|---|---|---|
| 2D-s1 | 0.6 | $3 \times 10^3$ | Triangular | 2-D static grid |
| 2D-s2 | 0.3 | $12 \times 10^3$ | | |
| 2D-s3 | 0.15 | $50 \times 10^3$ | | |
| 2D-a1 | 0.3 | $\sim 7 \times 10^3$ | | 2-D adaptive grid; a1 and a2 correspond to 1 and 2 levels of dynamic cell refinement from original grid 2D-s1 |
| 2D-a2 | 0.15 | $20 \times 10^3$ | | |
| 3D-s1 | 0.30 | $50 \times 10^3$ | Tetrahedral and pyramids | 3-D static grid |
| 3D-s2 | 0.15 | $\sim 150 \times 10^3$ | | |
| 3D-a1 | 0.15 | $\sim 150 \times 10^3$ | | 3-D adaptive grid, obtained with 1 level of dynamic cell refinement from original grid 3D-s1 |

Table 3
Description of the numerical parameters used for the investigation on the cell 'virtual' properties calculation

| Case | Cell 'virtual' properties calculation | Source term distribution and continuous phase variable interpolation | Continuous phase time step | Computational domain |
|---|---|---|---|---|
| 1/a | Yes | Cell-containing parcel | 1.E-5s | 2D-s3 |
| 1/b | No | Cell-containing parcel | 1.E-5s | 2D-s3 |
| 1/b | No | Cell-containing parcel | 1.E-7s | 2D-s3 |
| 2/a | Yes | Spatial distribution | 2.E-5s | 2D-s1 |
| 2/b | Yes | Spatial distribution | 2.E-5s | 2D-s2 |
| 2/c | Yes | Spatial distribution | 2.E-5s | 2D-s3 |
| 2/d | No | Spatial distribution | 2.E-5s | 2D-s2 |

The operating conditions correspond to cases 3 and 4 of Table 1.

continuous phase properties, re-calculated at each tracking time step, change because these are interpolated among new up-dated 'virtual' cell properties. Case 1/c further confirms that this methodology provides solution very close to that obtained by solving the full Navier–Stokes equations with the same time step as that of the Lagrangian parcels; obviously in this case virtual values are not considered but it requires ~20 times more CPU time in this particular case and thus not applicable in the majority of investigations.

Comparing the results between cases 1/a and 1/c the following conclusions are drawn. Shortly after the start of injection and between the time interval of $2 \times 10^{-5}$ s and $3 \times 10^{-5}$ s, which corresponds to 1/100 of a typical injection duration pulse, the differences between the two cases are less than 20% and 2% for the axial velocity and temperature flow fields, respectively. This can be considered an acceptable deviation from the actual solution for that limited time interval while at the same time guaranties stability

to the solver and significantly reduced calculation time. It ought to be mentioned here that results obtained with other time steps and reported later on in the paper also reveal that the solution obtained can be considered as time-step independent. Fig. 6 shows the temporal variation of the momentum exchanged between the two phases together with the momentum of the injected fuel; predictions obtained employing different grids are presented with and without the estimation of cell virtual properties. Fig. 6b corresponds to a detail of Fig. 6a, for the early stages of injection. On that plot, the vertical lines plotted correspond to the time where the gas phase motion is simulated. It is interesting to notice that in the case where the gas phase velocity seen by the parcel is not updated through the use of the cell virtual properties, the momentum exchanged may result in air velocity higher than that of the moving parcels, leading to the observed drop of the momentum exchange curve. Considering that injection velocity is increasing continuously during that period, this is obviously wrong. On the other hand, when the cell virtual properties are considered, then this not only prevents from non-physical values to be predicted but also results in effectively the same momentum exchanged as the grid is refined. Fig. 7 shows the temporal variation of the liquid penetration for the non-evaporating and evaporating cases 3 and 4 of Table 1, respectively. In this case the spatial interpolation/distribution method of Eq. (12) has been employed. The graphs show that the liquid penetration for the evaporating and non-evaporating sprays is over-predicted without the calculation of the cell 'virtual' properties although the source terms are distributed in the cells found in the vicinity of the droplet parcels. Fig. 7b suggests that the vapour penetration beyond the point where all liquid has been vaporised does not depend on the cell 'virtual' properties calculation.

### 2.7. Local grid refinement

Although it is generally accepted that cell refinement provides more accurate results, CFD codes might not be

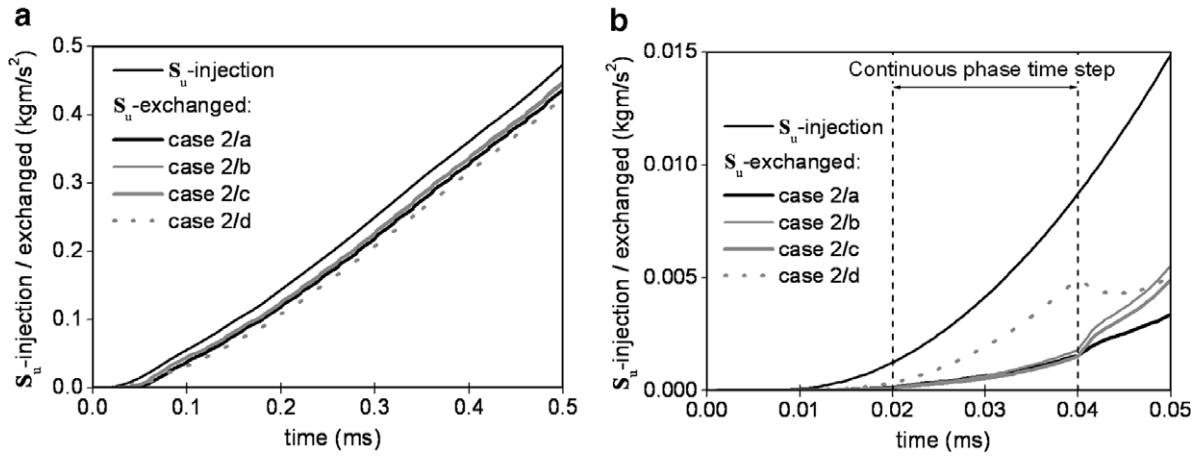


Fig. 6. (a) Effect of computational grid and cell-virtual properties estimation on predicted axial momentum exchanged between the liquid and gas phases of an evaporating spray up to 0.05 ms ASOI, (b) detail of (a); cases 2/a,b,c,d of Table 3.

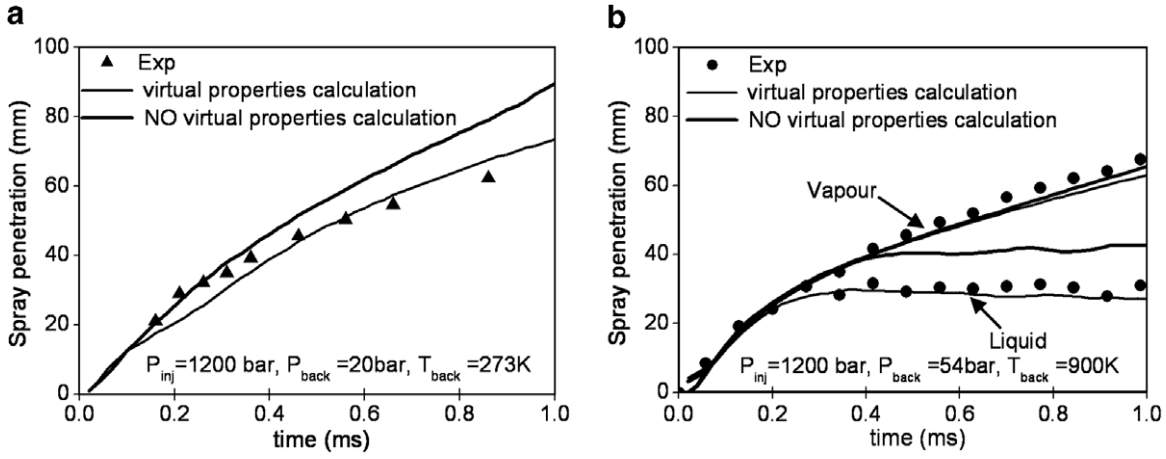


Fig. 7. Effect of cell-virtual properties estimation on temporal variation of liquid and vapour spray penetration under non-evaporating and evaporating conditions (a) case 3 of Table 1 and (b) case 4 of Table 1; the source terms are distributed within a region of 0.4 mm from the parcel centre.

able to handle very fine grids with cell size of the order of the parcel dimension due to the strong coupling between the two phases. Moreover, the computational time increases considerably with finer grids. These contradictory requirements suggest that adaptive local grid refinement in selected regions of the computational domain where and when it is needed may provide a reasonable compromise in terms of accuracy and computational time. This may be of practical importance in internal combustion engine simulations where the spray injection lasts only for a few crank angles of the total engine cycle. Fig. 8 shows three 2-D grids with minimum cell size from 0.6 mm down to 0.15 mm. These grids have been used to access the grid dependency of the simulation results while at the same time serve as reference for comparing the accuracy of the obtained solution and the corresponding computational time with grids of the same cell density but adaptively refined as part of the simulation. The adaptive local grid refinement technique employed here has been developed as part of the work within the authors' group and it is described in detail in Theodorakakos and Bergeles (2004); here results are presented for first time using this numerical methodology to the simulation of sprays. Remapping of the flow field variables in different grids is performed by interpolating the values of the variables in the cells of the grid of the previous time step closest to the cell of the new grid, by taking into account the distances between the nodes. The grid region dynamically refined corresponds to the cells where droplet parcels are present at the beginning of a new continuous phase time step. The droplet parcel locations are recorded at each time step and the cells to be split are identified; then a new refined grid is created. Fig. 9 shows the refinement (split) of four different cell types used here (tetrahedron, hexahedron, and pyramid and prism) to smaller ones. The principle adopted here for the split is based on the concept that any cell face should split only in similar ones (i.e. the triangle splits in triangles and the rectangle in rectangles). Successive refinement of any cell can be performed; here up to three levels of grid refinement have been tested. In Fig. 10, the 2-D grids with adaptive cell refinement in the region of the spray development are shown at three time steps

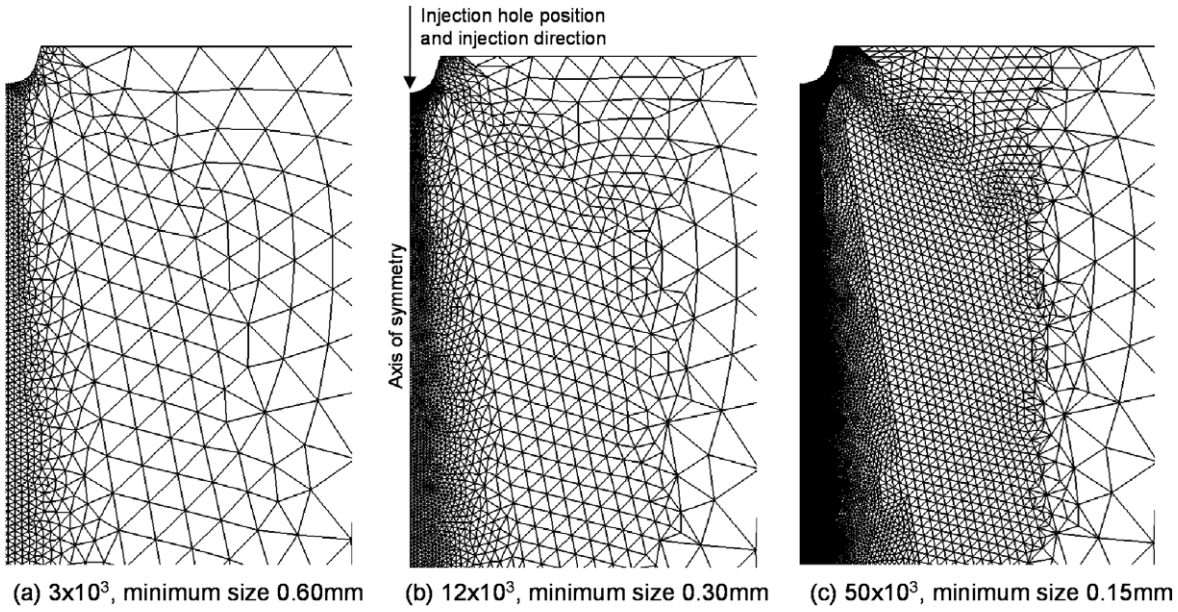


Fig. 8. Sub-domain of the (a) 2D-s1, (b) 2D-s2 and (c) 2D-s3 computational grids; the minimum cell length in the axial direction is also indicated.

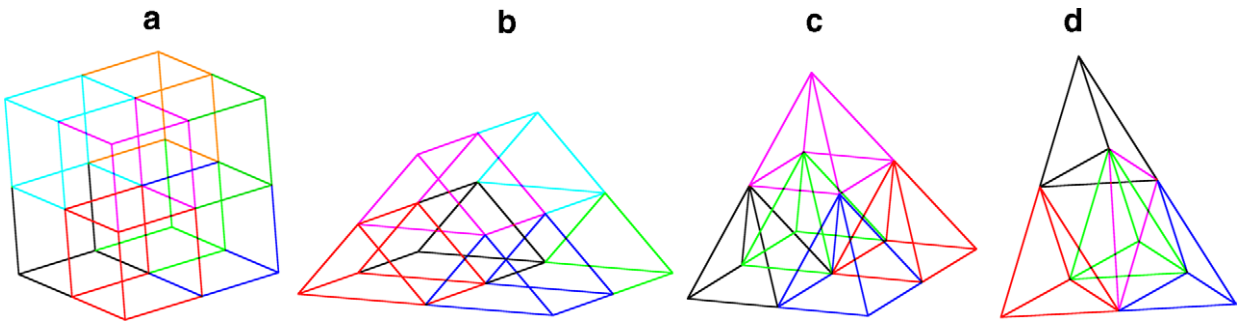


Fig. 9. Schematic showing the split of cells into elementary ones (a) hexahedron splits in eight hexahedrons, (b) prism splits in eight prisms, (c) pyramid splits in six pyramids and four tetrahedrons and (d) tetrahedron splits in eight tetrahedrons.

during the spray development, while in Fig. 11 the 3-D static and dynamic grids used are shown; Fig. 11b and c present the 3-D computational domains obtained by one level of refinement of the coarse grid shown in Fig. 11a. The refined cells shown in Fig. 11b correspond to the location of all parcels present in the calculation while in Fig. 11c the refined cells are those belonging to the spray tip region. The notation used with reference to these grids is tabulated in Table 2.

## 3. Results and discussion

This section of the paper presents the results obtained using the above described model for simulating the development of Diesel sprays injected from an axi-symmetric single-hole cavitating nozzle. The set of experimental measurements used for model validation include the temporal variation of the liquid and vapour penetration reported by König and Blessing (2003); the test cases selected for presentation here are summarised in Table 1. Two-phase internal nozzle flow calculations performed using rail pressure measurements and reported in Giannadakis et al. (2004) have provided the injection conditions used as inputs to the Eulerian–Lagrangian spray model. Injection was taking place against pressurised $N_2$. Spray simulations have been performed under both non-evaporating and evaporating conditions. The air thermodynamic conditions were 20 bar and 273 K pressure and temperature, respectively, for the non-evaporating case and 54 bar and 900 K for the evaporating case. These two cases have been selected in such a way that the air density was kept constant; more details about the nozzle characteristics and the test cases operating can be found in Tonini (2006), together with the discussion on the selection of the spray

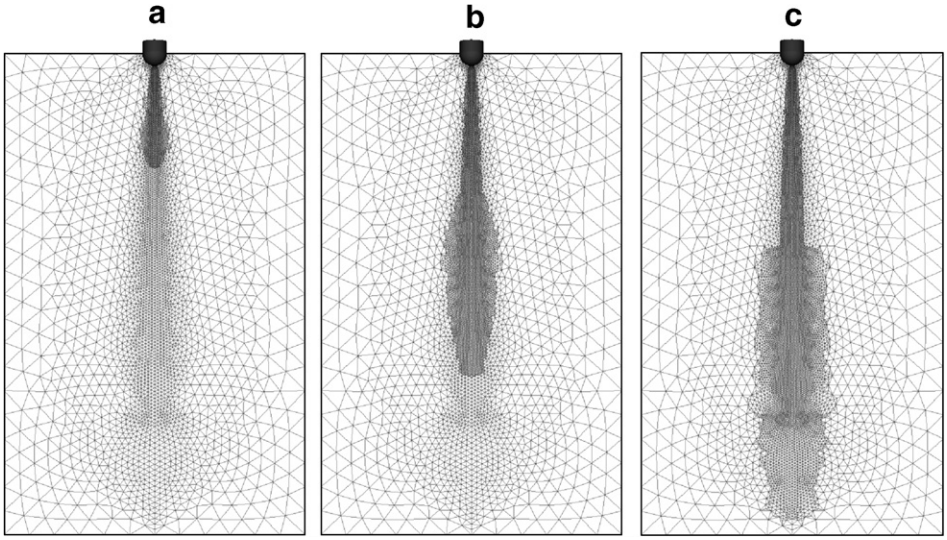


Fig. 10. 2-D axis-symmetric adaptive numerical grid at three time instances calculated during the spray development at (a) 0.1 ms with $5 \times 10^3$ cells, (b) 0.5 ms with $8 \times 10^3$cells and (c) 1.0 ms with $10 \times 10^3$ cells.

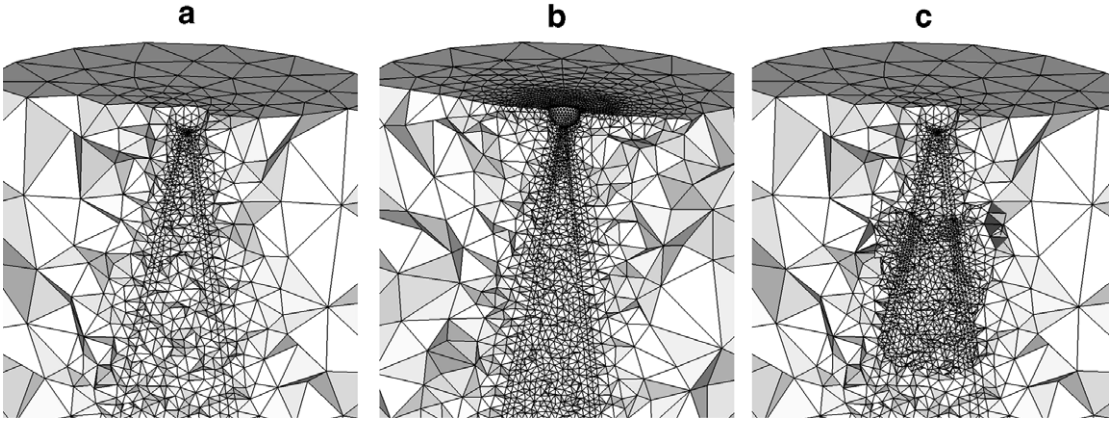


Fig. 11. 3-D static and adaptive numerical grids used for the simulation of the spray development (a) $50 \times 10^3$ cells, (b) $240 \times 10^3$ cells, (c) $50 \times 10^3$ cells with automatic local refinement at the spray tip.

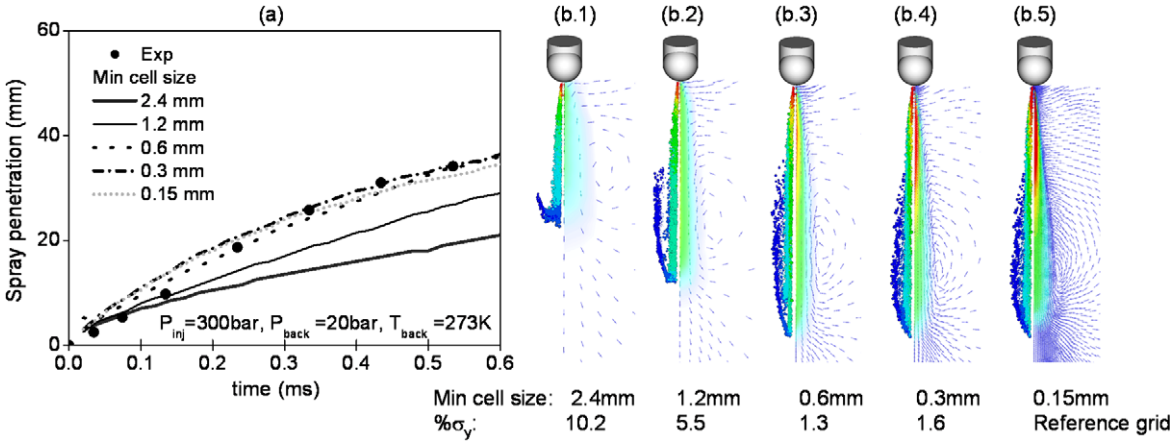


Fig. 12. Effect of grid density on (a) temporal variation of spray tip penetration and (b) predicted spray structure; case 2 of Table 1.

sub-models used for the purposes of the present investigation.

The first set of results to be presented refers to the sensitivity of the predictions to the numerical grid density. As mentioned, unstructured 2-D axis-symmetric and 3-D grids, with different levels of static and dynamic cell refinements have been used. Fig. 12a shows the effect of grid refinement on the temporal development of the tip penetration of the non-evaporating spray injected with a nominal rail pressure of 300 bar (case 2 of Table 1), while Fig. 12b shows the calculated spray structure 0.6 ms after start of injection; on that graph, the minimum cell size used is indicated. This lowest injection pressure case has been specifically selected since it should be the less grid-dependent one. The coarser grid has a minimum cell size of 2.4 mm which is then successively refined in the region of the spray development; the grid spacing of the finer grid used is 0.15 mm. As can be seen in Fig. 12a, model predictions significantly change as the grid is refined, but they converge to values close to the experimental ones while no differences can be realised for the most two refined grids. This is also clear in the images of Fig. 12b which confirm that the simulations performed with successive grid refinement predict the same spray tip penetration and also almost identical spray structures. Results obtained for increased injection pressure of 1200 bar are shown in Figs. 13–17 both under non-evaporating (case 3) and evaporating (case 4) conditions. Fig. 13 shows the comparison between model predictions and experimental data using the 2-D static and adaptive grids; similarly to the previous case of lower injection pressure, the predicted liquid penetration converges to the experimental data. Particularly for the non-evaporating case, the results confirm that even the coarser computational domain used (in this case with 0.6 mm minimum cell size) in this test case allows reasonably accurate predictions. On the other hand, more visible differences exist between the predicted vapour penetration profiles for the evaporating spray case. This is an expected result, since the vapour penetration is a result of the induced by the spray air motion, which convects the vaporised fuel downstream from the injector nozzle location. The graphs reveal that dynamically refined domains guarantee the accuracy

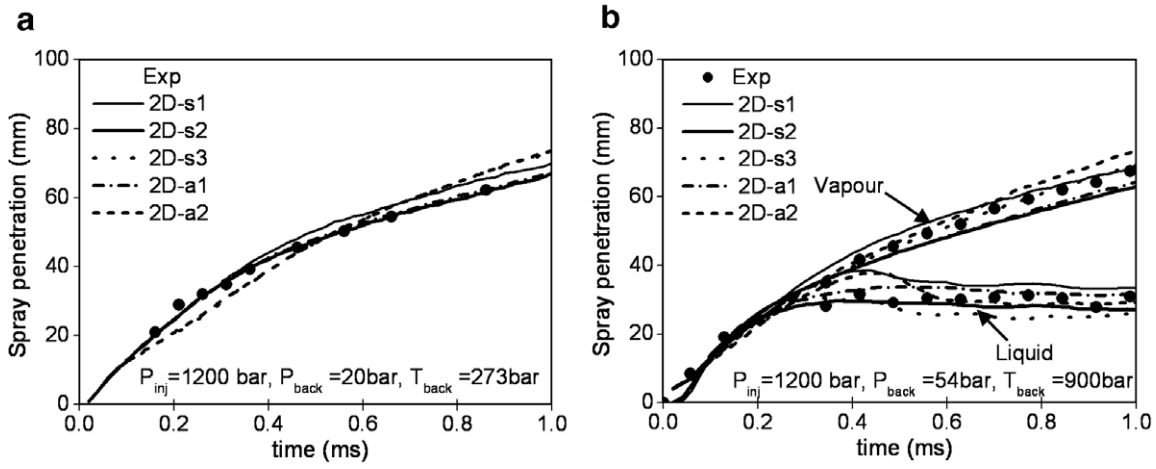


Fig. 13. Effect of 2-D numerical grid on the temporal variation of liquid and vapour penetration under non-evaporating and evaporating conditions; (a) case 3 of Table 1 and (b) case 4 of Table 1.

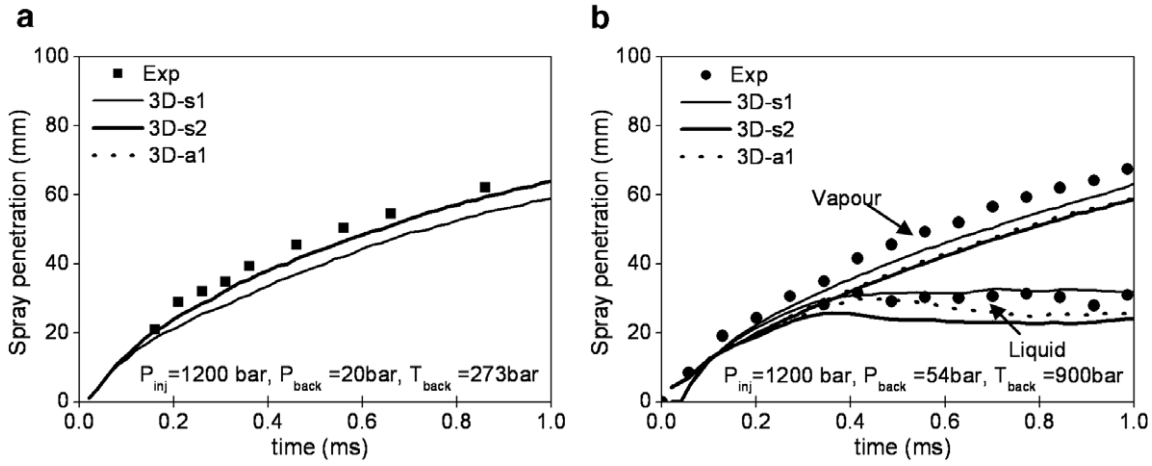


Fig. 14. Effect of 3-D numerical grid on temporal variation of liquid and vapour penetration under non-evaporating and evaporating conditions; (a) case 3 of Table 1 and (b) case 4 of Table 1.

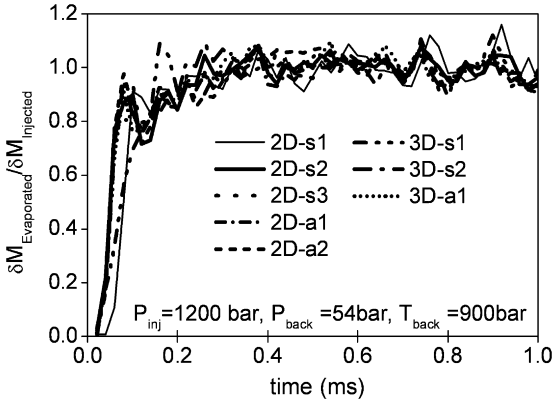


Fig. 15. Effect of 2-D and 3-D numerical grid on the temporal variation of non-dimensional evaporation rate of the evaporating spray; case 4 of Table 1.

of static grid with the same cell density in the region of spray development, but obviously at reduced computational cost. Fig. 14 presents the grid effect for the same conditions of Fig. 13 but this time using 3-D meshes. The first simulation has been performed using the reference coarse grid consisting of 50,000 cells. Successively, a second simulation has been performed by activating one level of dynamic cell refinement in the region of spray development. This refined grid consists of about 150,000 cells. The results reveal that the increase of cell density leads to higher liquid penetration for the non-evaporating spray. A different trend is observed in case of evaporation, when the liquid stops at a closer distance from the nozzle hole, due to the increased evaporation rate predicted at the initial stage of the injection period. Again, similar accuracy is predicted with dynamically refined and static grids, provided that the cell density is the same. Fig. 15 shows the effect of grid density on the temporal development of the fuel vaporisation rate, normalised with the instantaneous injection rate, for the same operating conditions of Figs. 13 and 14. The fluctuations in the evaporation rate are related to the fluctuation in the injection flow rate. This ratio becomes almost equal to one approximately 0.25 ms

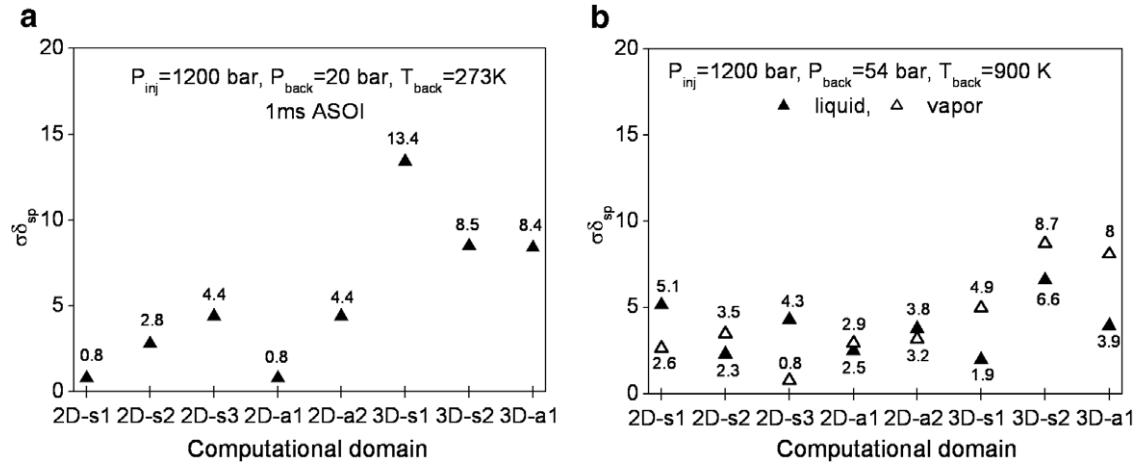


Fig. 16. Standard deviation between predicted and measured liquid and vapour penetration for the static and adaptive 2-D and 3-D numerical grids used, under non-evaporating and evaporating conditions; (a) case 3 of Table 1 and (b) case 4 of Table 1.

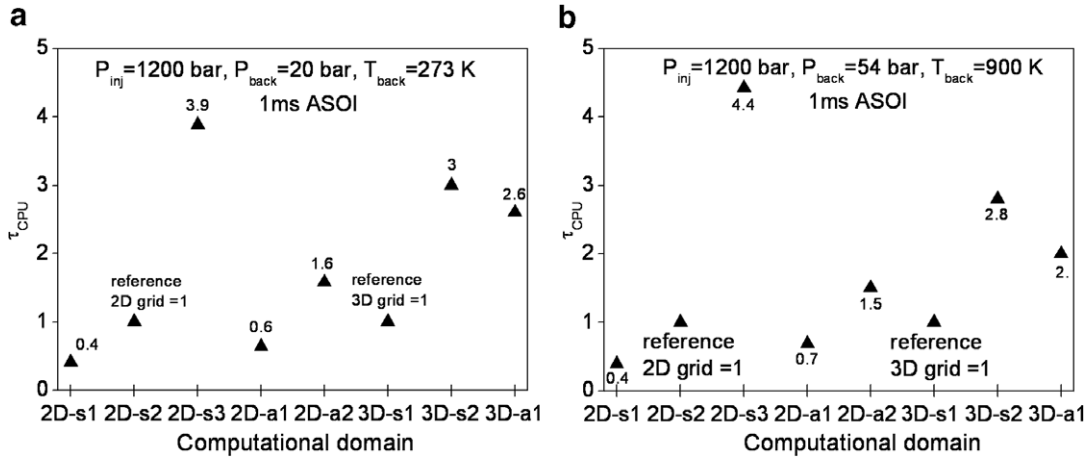


Fig. 17. Normalised calculation time relative to the reference-case, using static and adaptive 2-D and 3-D numerical grids, for non-evaporating and evaporating conditions; (a) case 3 of Table 1 and (b) case 4 of Table 1.

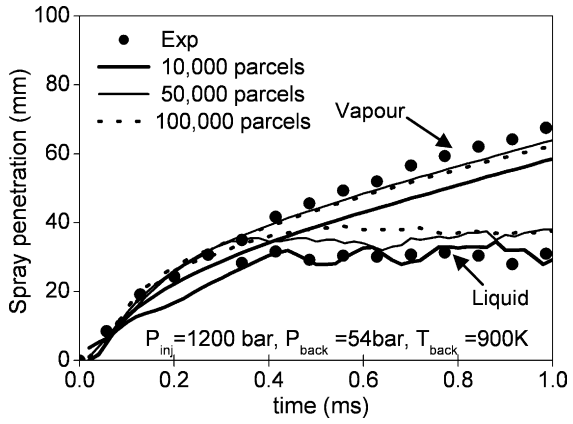


Fig. 18. Effect of number of parcels injected on temporal variation of liquid and vapour penetration of an evaporating spray; case 4 of Table 1.

after start of injection, almost independently from the grid used. This implies that after that time the fuel vaporisation rate will be equal to the fuel injected and thus it is expected that, after a short delay, liquid penetration will freeze, in agreement with the experimental data.

In order to quantify the differences between the experimental data and the model predictions, the standard deviation of the liquid penetration, predicted using the different numerical domains, from the value obtained with the finest grid, taken as the reference case, is calculated according to the following equation:

$$\sigma\delta_{\mathrm{sp}_i} = \sqrt{\frac{1}{N_{\Delta t}}\sum_{n=1}^{N\Delta t}\left(\mathrm{sp}_i(t) - \overline{\mathrm{sp}}(t)\right)^2} \tag{30}$$

where $\mathrm{sp}_i(t)$ represents the predicted spray penetration at the time $\Delta t$ using the grid $i$, $\overline{\mathrm{sp}}(t)$ the corresponding experimental value and $N_{\Delta t}$ is the total number of time steps in the averaging interval. The corresponding values are plotted in Fig. 16 for a time interval lasting up to 1 ms from the start of injection. The results show that the standard deviation for all the conditions investigated is less than 5% for 2-D calculations, and about 8.5% for refined 3-D

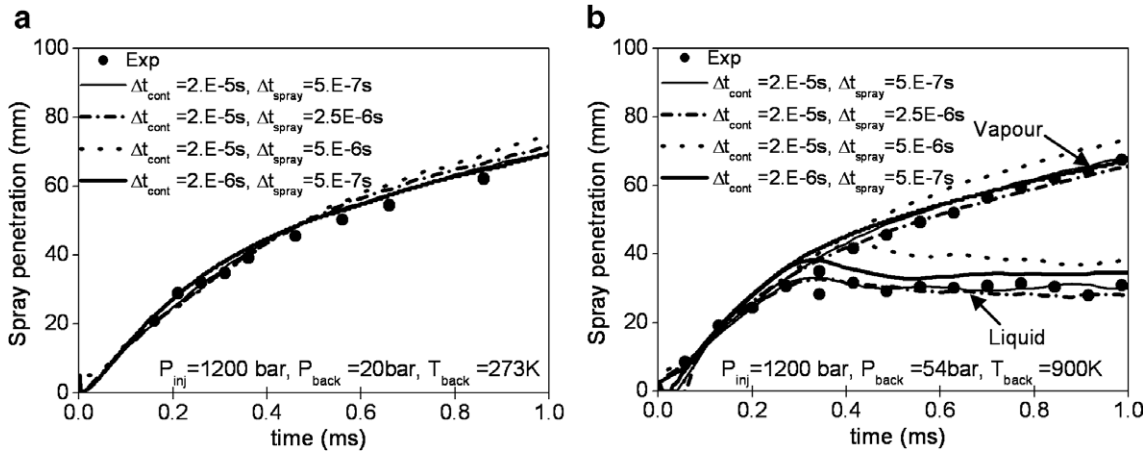


Fig. 19. Effect of time step on temporal variation of liquid and vapour spray penetration under non-evaporating and evaporating conditions; (a) case 3 of Table 1 and (b) case 4 of Table 1.

grids under non-evaporating conditions; the initial 3-D grid results to predictions that substantially deviate from the experiments more than 13%. Differences are smaller for the evaporating sprays and do not exceed 4% for the 2-D calculations and 4–8% for the 3-D cases.

The implementation of adaptive grid refinement is expected to reduce the computational time required for the simulation. This can be seen in Fig. 17, which presents the normalised CPU (Central Power Unit) time for all the simulations presented in Fig. 16, taking as reference value the 2D-s2 and 3D-s1 grids for the 2-D and 3-D cases, respectively. The results show that the CPU time for 2-D meshes reduces down to more than half when adaptive grid refinement is used compared to the static (pre-refined) grid having the same level of refinement. This reduction is about 30% in case of 3-D grids. These conclusions are valid for both non-evaporating and evaporating conditions.

The next few figures to be presented assess the effect of additional numerical parameters on model predictions. These are the number of computational parcels used to resolve the spray, the discretisation scheme used for the numerical solution of the gas motion and the time step of the dispersed and continues phases. Fig. 18 shows that the liquid and vapour penetrations are not considerably affected by the total number of parcels injected, which is varied from 10,000 up to 100,000. Fig. 19 shows the sensitivity of the model prediction on the selection of the time step used for the solution of the continuous and dispersed phases. Four combinations of continuous and dispersed phase time steps have been tested. In the first three cases the time step for the dispersed phase was set equal to $5 \times 10^{-7}$ s, $2.5 \times 10^{-6}$ s and $5 \times 10^{-6}$ s, while the time step for the continuous phase was fixed at $2.5 \times 10^{-6}$ s. In the last case the time step for the dispersed and continuous phase have been set equal to $5 \times 10^{-7}$ s and $2–10^{-6}$ s, respectively. The results show that the smaller tracking time step allows more accurate predictions to be obtained, while reduction of the continuous phase time step does not affect the predictions significantly. The results presented in Fig. 20 reveal that the computational results are not significantly affected by the discretisation scheme used. This is mainly due to the fact that the flow is driven by the momentum exchange between the two phases while the velocity component in the direction of the spray is two orders of magnitude greater from the other two. Thus, numerical diffusion effects are playing only a minor role in this particular flow development. Finally Fig. 21 and Table 4 summarise the results from the numerical investigation presented in this section, both for the non-evaporating and evaporating conditions. The percentage standard deviation of the predicted liquid and vapour penetration from the experimental measurements, calculated according to Eq. (30) is shown. Deviation above 10% is calculated only for 3-D non-evaporating spray simulation using the coarse grid. Moreover, if cell 'virtual' properties during the parcel sub-cycles are not considered, which results in the over-prediction of the source terms from mass, momentum and energy exchange, then this consequently results to an over-estimation of liquid penetration by more than 10%, for both the non-evaporating and evaporating sprays.

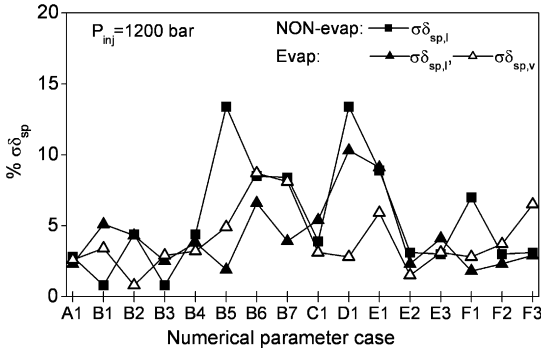


Fig. 21. Standard deviation between predictions and measurements for the liquid and vapour penetration under both non-evaporating and evaporating conditions; case index as described in Table 4.

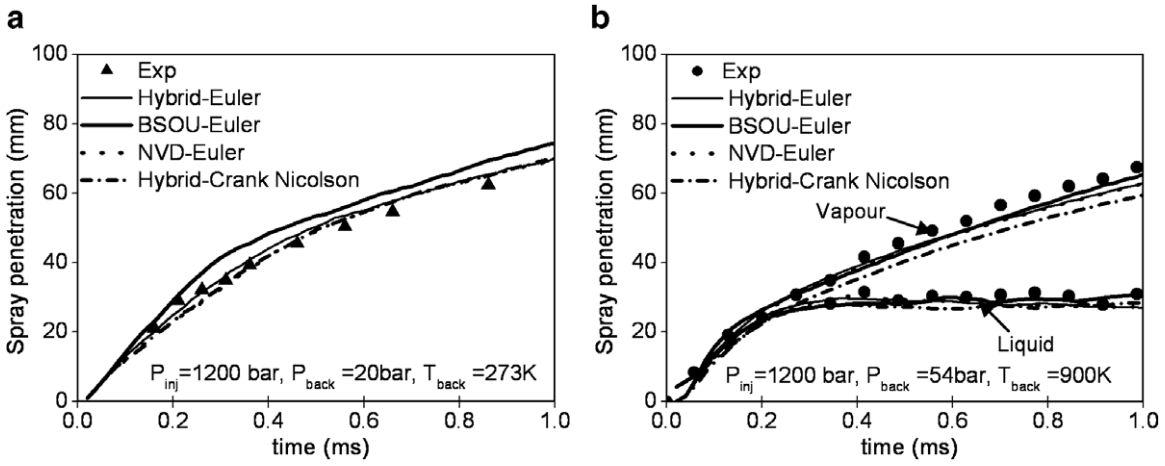


Fig. 20. Effect of discretisation scheme of the gas-phase equations on temporal variation of liquid and vapour penetration under non-evaporating and evaporating conditions; (a) case 3 of Table 1 and (b) case 4 of Table 1.

Table 4
Summary of the numerical parameters effect on the predicted liquid and vapour penetration under non-evaporating and evaporating conditions

| Numerical parameter | Description | Case | Case 3 | Case 4 | |
|---|---|---|---|---|---|
| | | | $\sigma\delta_{sp,I}$ | $\sigma\delta_{sp,I}$ | $\sigma\delta_{sp,v}$ |
| Standard settings | Grid: 2D-s2; $R_{interp}$/distr = 0.4 mm; with virtual properties; $\Delta t_{cont}$ = 2.E-5s, $\Delta t_{spray}$ = 5.E-7s; discretisation method: Hybrid-Euler | $A_1$ | 2.8 | 2.3 | 2.6 |
| Grid effect | 2D-s1 | $B_1$ | 0.8 | 5.1 | 3.4 |
| | 2D-s3 | $B_2$ | 4.4 | 4.3 | 0.8 |
| | 2D-a1 | $B_3$ | 0.8 | 2.5 | 2.9 |
| | 2D-a2 | $B_4$ | 4.4 | 3.8 | 3.2 |
| | 3D-s1 | $B_5$ | 13.4 | 1.9 | 4.9 |
| | 3D-s2 | $B_6$ | 8.5 | 6.6 | 8.7 |
| | 3D-a1 | $B_7$ | 8.4 | 3.9 | 8.1 |
| Effect of distribution distance | $R_{interp/distr}$ = parcel diameter | $C_1$ | 3.9 | 5.4 | 3.1 |
| Effect of virtual properties | NO virtual properties | $D_1$ | 13.4 | 10.3 | 2.8 |
| Effect of time step | $\Delta t_{cont}$ = 2.E-5s, $\Delta t_{spray}$ = 5.E-6s | $E_1$ | 8.9 | 9.1 | 5.9 |
| | $\Delta t_{cont}$ = 2.E-5s, $\Delta t_{spray}$ = 2.5E-6s | $E_2$ | 3.1 | 2.3 | 1.5 |
| | $\Delta t_{cont}$ = 2.E-6s, $\Delta t_{spray}$ = 5.E-7s | $E_3$ | 3.0 | 4.1 | 3.1 |
| Effect of discretisation method | BSOU-Euler | $F_1$ | 7.0 | 1.8 | 2.8 |
| | NVD-Euler | $F_2$ | 3.0 | 2.3 | 3.7 |
| | Hybrid-Crank–Nicholson | $F_3$ | 3.1 | 2.9 | 6.5 |

Cases 3 and 4 of Table 1.

## 4. Concluding remarks

A numerical methodology for dense spray calculations has been presented and assessed against experimental data. The originality of the numerical model proposed here consists of the simultaneous employment of three numerical methodologies, namely (i) distribution of the source terms expressing the mass, momentum and energy coupling between the two phases into a several cells found in the vicinity of the droplet, (ii) estimation of the airflow properties at the time scale of droplet movement through introduction of so-called 'virtual properties' which prevent from non-physical exchange source terms to be calculated and (iii) application of adaptive local grid refinement in the area of liquid injection, which gives the desired grid resolution without compromising in computational time. The model can be easily implemented in existing CFD codes without the need to switch to Eulerian–Eulerian calculations while at the same time can result in grid-independent solution as the grid is successively refined. The mass, momentum and energy exchanged between the liquid and gaseous phases is performed through use of weighting functions which distribute them in a conservative way in a number of cells found in the vicinity of the droplet; this resolves numerical as well as physical problems realised when the volume available between the two phases is limited to the cell-containing parcel and whose volume may become comparable to that of the cell volume. The two orders of magnitude difference in the time scale required for resolving the development of the two phases imposes the adoption of a semi-implicit scheme of updating the flow variables of the Eulerian phase realised by the moving particles during their successive pass from a computational cell. During the time interval between successive solutions of the air motion, the exchange of mass, momentum and energy between the two phases is controlled within physically allowed limits; this was achieved by estimation of 'cell-virtual' flow variables which are updated during the motion of every droplet parcel. Computational time was significantly reduced through use of the adaptive grid refinement performed only in the area of spray development, and which changes dynamically together with the penetrating fuel plume. The developed dense-particle fluid dynamics model was assessed against experimental data of high-pressure Diesel sprays injected from a single-hole cavitating nozzle design under both non-evaporating and evaporating conditions and using as initial conditions simulation results of the internal nozzle flow. Predictions converge close to the experimental values with successive levels of grid refinement without the need to use Eulerian flow models in the near nozzle region. The standard deviation between measured values for the liquid and vapour penetration and model predictions was less than 5% for the finer grids. Model predictions have been obtained using different spatial and temporal discretisation schemes implemented to solve the continuous and dispersed phase governing equations. In addition, the effect of different interpolation/distribution methods, adaptive time step and number of computational parcels used to represent the droplet cloud have been investigated. These parameters may result in up to 5% difference between model predictions while in any case the maximum deviation between model predictions and experiments was less than 8% for medium refined 3-D grids suitable for engine calculations. The results obtained highlight the significant

improvements of the method compared to the standard Lagrangian methodology, in terms of accuracy, numerical stability and dependency on the grid resolution.

## Acknowledgement

The authors would like to acknowledge the contribution of Dr. Giannadakis for the cavitating nozzle flow calculations, which provide the injection conditions to the spray modelling. DaimlerChrysler AG is acknowledged for the provision of the experimental data used for model validation and for the permission to use them for the purposes of this publication.

## References

Abraham, J., 1997. What is adequate resolution in the numerical computation of transient jets? SAE 970051.

Abraham, J., Magi, V., 1999. A virtual liquid source (VLS) model for vaporizing Diesel sprays. SAE 1999-01-0911.

Aggarwal, S.K., Mongia, H.C., 2002. Multicomponent and high-pressure effects on droplet vaporization. Journal of Engineering for Gas Turbines and Power 124, 248–255.

Alajbegovic, A., Drew, D.A., Lahey, R.T., 1999. An analysis of Phase distribution and turbulence in dispersed particle/liquid flows. Chemical Engineering Communications 174, 85–133.

Aneja, R., Abraham, J., 1998. How far does the liquid penetrate in a diesel engine: computed results vs. measurements? Combustion Science and Technology 138, 233–255.

Arcoumanis, C., Gavaises, M., 1998. Linking the nozzle flow with spray characteristics in a Diesel fuel injection system. Atomization and Sprays 8, 179–197.

Arcoumanis, C., Gavaises, M., French, B., 1997. Effect of fuel injection processes on the structure of diesel sprays. SAE 970799.

Barroso, G., Schneider, B., Boulouchos, K., 2003. An extensive parametric study on diesel spray simulation and verification with experimental data. SAE 2003-01-3230.

Beard, P., Duclos, J.M., Habchi, C., Bruneaux, G., Mokkadem, K., Baritaud, T., 2000. Extension of Lagrangian–Eulerian spray modelling: application to high pressure evaporating diesel sprays. SAE 2000-01-1893.

Beau, P.-A., Funk, M., Lebas, R., Blokkeel, G., 2005. Applying quasi-multiphase model to simulate atomization processes in diesel engines: modelling of the slip velocity. SAE 2005-01-0220.

Beck, J.C., Watkins, A.P., 2004. The simulation of fuel sprays using the moments of the drop number size distribution. International Journal of Engine Research 5, 1–21.

Bensler, H., Bühren, F., Samson, E., Vervisch, L., 2000. 3-D CFD Analysis of the combustion process in a DI diesel engine using a flamelet model. SAE 2000-01-0662.

Bianchi, G., Minelli, F., Scardovelli, R., Zaleski, S., 2007. 3D large-scale simulation of the high-speed liquid jet atomisation. SAE 2007-01-0244.

Bianchi, G., Pelloni, P., Toninel, S., Suzzi, D., Paganelli, D., 2004. A 2-D simulation method for computing droplet size spectrum during the atomisation of high-speed liquid jets. ASME atomisation of high-speed liquid jets. In: Proceedings of ASME ICE04 Fall Technical Conference, ICEF2004-848.

Bianchi, G., Pelloni, P., Toninel, S., Zaleski, S., Leboissetier, A., Scardovelli, R., 2005. A quasi-direct 3-D simulation of the atomisation of high-speed liquid jets. In: Proceedings of ASME ICES05 Spring Technical Conference, ICES2005-1067.

Canakci, M., Reitz, R.D., 2003. Experimental optimization of a DI-HCCI-gasoline engine using split injections with fully-automated micro-genetic algorithms. International Journal of Engine Research 4, 47–60.

Caretto, L.S., Gosman, A.D., Patankar, S.V. and Spalding, D.B., 1972. Two calculation procedures for steady, three-dimensional flows with recirculation. In: Proceedings of the Third International Conference on Numerical Methods in Fluid Dynamics, Paris, France.

Dukowicz, J.K., 1980. A particle-fluid numerical model for liquid sprays. Journal of Computational Physics 35, 229–253.

Feng, Z.G., Michaelides, E.E., 2001. Drag coefficients of viscous spheres at intermediate and high Reynolds numbers. Journal of Fluids Engineering – Transactions of the ASME 123, 841–849.

Gavaises, M., Theodorakakos, A., Bergeles, G., Brenn, G., 1996. Evaluation of the effect of droplet collisions on spray mixing. Proceeding of the Institution of Mechanical Engineers 210, 465–475.

Giannadakis, E., Gavaises, M., Roth, H., Arcoumanis, C., 2004. Cavitation Modelling in Single-Hole Diesel Injector Based on Eulerian–Lagrangian Approach. In: Proceedings of the THIESEL International Conference on Thermo- and Fluid Dynamic Processes in Diesel Engines, Valencia, Spain.

Golovitchev, V.I., Nordin, N., 2001. Detailed chemistry spray combustion model for the KIVA code. In: Proceedings of the 11th International Multidimensional Engine Modeling User's Group Meeting at the SAE Congress, Detroit, pp. 1–6.

Gosman, A.D., 1999. State of the art of multi-dimensional modelling of engine reacting flows. Oil & Gas Science and Technology 54, 149–159.

Hohmann, S., Renz, U., 2003. Numerical simulation of fuel sprays at high ambient pressure: the influence of real gas effects and gas solubility on droplet vaporisation. International Journal of Heat and Mass Transfer 46, 3017–3028.

Huh, K.Y., Gosman, A.D., 1991. A phenomenological model of diesel spray atomisation. In: Proceedings of the International Conference on Multiphase Flows, Tsukuba, Japan.

Issa, R.I., 1986. Solution of implicitly discretised fluid flow equations by operator splitting. Journal of Computational Physics 62, 40–65.

Jasak, H., Weller, H.G., Gosman, A.D., 1999. High resolution NVD differencing scheme for arbitrarily unstructured meshes. International Journal for Numerical Methods in Fluids 31, 431–449.

König, G., Blessing, M., 2003. Database on spray characteristics. I-LEVEL Confidential Report, Daimlerchrysler AG.

Launder, B.E., Spalding, D.B., 1972. Lectures in Mathematical Models of Turbulence. Academic Press, London.

Lebas, R., Blokkeel, G., Beau, P.-A., Demoulin, F.-X., 2005. Coupling vaporization model with Eulerian–Lagrangian spray atomization (ELSA) model in diesel engine conditions. SAE 2005-01-0213.

Lippert, A.M., Chang, S., Are, S., Schmidt, D.P., 2005. Mesh independence and adaptive mesh refinement for advanced engine spray simulations. SAE 2005-01-0207.

O'Rourke, P.J., 1981. Collective drop effects on vaporizing liquid sprays. PhD Thesis, Princeton University.

O'Rourke, P.J., 1989. Statistical properties and numerical implementation of a model for droplet dispersion in turbulent gas. Journal of Computational Physics 83, 345–360.

Papadakis, G., Bergeles, G., 1995. A locally modified second order upwind scheme for convection terms discretisation. International Journal of Numerical Methods in Heat and Fluid Flow 5, 49–62.

Platzer, E., Sommerfeld, M., 2002. Modelling of Turbulent Atomisation with a Combined Euler/Lagrangian Approach: Starting with a Two-fluid Model in the Dense Spray Region. ILASS-Europe 2002, Zaragoza, Spain.

Reitz, R.D., Bracco, F.V., 1982. Mechanism of atomisation of a liquid jet. Physics of Fluids 25, 1730–1741.

Rhie, C.M., Chow, W.L., 1983. A numerical study of the turbulent flow past an isolated airfoil with trailing edge separation. AIAA Journal 21, 1525–1532.

Sazhin, S.S., 2006. Advanced models of fuel droplet heating and evaporation. Progress in Energy and Combustion Science 32, 162–214.

Schmidt, D.P., Rutland, C.J., 2000. A new droplet collision algorithm. Journal of Computational Physics 164, 62–80.

Schmidt, D.P., Rutland, C.J., 2003. Reducing grid dependency in droplet collision modeling. Journal of Engineering for gas turbines and power, 125.

Steiner, R., 2004. 3D-combustion simulation: potentials, modelling and application Issues. In: Proceedings of the 10th Diesel Engine Emissions Reduction Conference, Coronado, California.

Sterno, N., Greeves, G., Tullis, S., Jiang, X., Zhao, H., 2006. Simulation of the air/fuel mixing of an HSDI diesel engine. Part 1: a new dense spray vapour coupling submodel. Proceedings of the I MECH E Part D Journal of Automobile Engineering 220, 1793–1805.

Subramaniam, S., O'Rourke, P.J., 1998. Numerical convergence of the KIVA-3 code for sprays and its implications for modelling. Los Alamos Unclassified Report LAUR 98-5465.

Theodorakakos, A., Bergeles, G., 2004. Simulation of sharp gas–liquid interface using VOF method and adaptive grid local refinement around the interface. International Journal for Numerical Methods in Fluids 45, 421–439.

Tomiyama, A., 2002. Some attempts for the improvement of computational bubble dynamics. In: Proceedings of the 10th Workshop on Two-Phase Flow Predictions, Merseburg, Germany, pp. 125–136.

Tonini, S., 2006. Fuel spray modelling in direct injection diesel and gasoline engines. PhD Thesis, City University London.

Tristano, J.R., Chen, Z., Hancq, D.A., Kwok, W., 2003. Fully automatic adaptive mesh refinement integrated into the solution process. In: Proceedings of the 12th International Meshing Roundtable, Sandia National Laboratories, pp. 307–314.

Trujillo, M.F., Torres, D.J., O'Rourke, P.J., 2004. High-pressure multicomponent liquid sprays: departure from ideal behaviour. International Journal of Engine Research 5, 229–246.

v. Berg, E., Alajbegovic, A., Tatschl, R., Krüger, C., Michels, U., 2001. Multiphase modelling of diesel sprays with the Eulerian/Eulerian approach. In: Proceedings of the 17th ILASS Europe Conference, Zürich.

Vallet, A., Burluka, A.A., Borghi, R., 2001. Development of a Eulerian model for the "atomization" of a liquid jet. Atomisation and Sprays 11, 619–642.

Versaevel, P., Motte, P., Wieser, K., 2000. A new 3D model for vaporizing diesel sprays based on mixing-limited vaporization. SAE 2000-01-0949.

Villiers, E.D., Gosman, A.D., Weller, H.G., 2004. Large eddy simulation of primary Diesel spray atomisation. SAE 2004-01-0100.

Wan, J., Kocak, S. and Shephard, M.S., 2003. Automated adaptive forming simulations. In: Proceedings of the 12th International Meshing Roundtable, Sandia National Laboratories, pp. 323–334.

Wan, Y.P., Peters, N., 1997. Application of the cross-sectional average method to calculations of the dense spray region in a Diesel Engine. SAE 972866.